Published March 2, 2009

Mammalian end binding proteins control persistent microtubule growth

Yulia Komarova,[1] Christian O. De Groot,[2] Ilya Grigoriev,[3] Susana Montenegro Gouveia,[3] E. Laura Munteanu,[5] Joseph M. Schober,[1] Srinivas Honnappa,[2] Rubén M. Buey,[2] Casper C. Hoogenraad,[4] Marileen Dogterom,[5] Gary G. Borisy,[1] Michel O. Steinmetz,[2] and Anna Akhmanova[3]

[1]Department of Cell and Molecular Biology, Northwestern University Medical School, Chicago, IL 60611
[2]Biomolecular Research, Structural Biology, Paul Scherrer Insititut, CH-5232 Villigen PSI, Switzerland
[3]Department of Cell Biology and [4]Department of Neuroscience, Erasmus Medical Center, 3000 CA Rotterdam, Netherlands
[5]FOM Institute for Atomic and Molecular Physics (AMOLF), Kruislaan 407, 1098 SJ Amsterdam, Netherlands

End binding proteins (EBs) are highly conserved core components of microtubule plus-end tracking protein networks. Here we investigated the roles of the three mammalian EBs in controlling microtubule dynamics and analyzed the domains involved. Protein depletion and rescue experiments showed that EB1 and EB3, but not EB2, promote persistent microtubule growth by suppressing catastrophes. Furthermore, we demonstrated in vitro and in cells that the EB plus-end tracking behavior depends on the calponin homology domain but does not require dimer formation. In contrast, dimerization is necessary for the EB anti-catastrophe activity in cells; this explains why the EB1 dimerization domain, which disrupts native EB dimers, exhibits a dominant-negative effect. When microtubule dynamics is reconstituted with purified tubulin, EBs promote rather than inhibit catastrophes, suggesting that in cells EBs prevent catastrophes by counteracting other microtubule regulators. This probably occurs through their action on microtubule ends, because catastrophe suppression does not require the EB domains needed for binding to known EB partners.

Introduction

Microtubules (MTs) are intrinsically polar filaments with two structurally and functionally distinct ends, the plus- and the minus-end (Desai and Mitchison, 1997; Howard and Hyman, 2003). In cells, MT minus-ends are predominantly stable and often associated with the MT organizing center, whereas MT plus-ends spontaneously switch between phases of growth and shrinkage (Desai and Mitchison, 1997; Howard and Hyman, 2003). Growing MTs accumulate at their plus-ends multiple structurally unrelated factors collectively termed MT plus-end tracking proteins, or +TIPs (Schuyler and Pellman, 2001; Akhmanova and Steinmetz, 2008).

The most conserved and ubiquitous +TIPs are end binding proteins (EBs) (Tirnauer and Bierer, 2000). These are relatively small dimeric proteins which contain an N-terminal calponin homology (CH) domain, responsible for the interaction with MTs, a linker region of unknown function, and a C-terminal coiled coil domain that extends into a four-helix bundle, required for dimer formation (for review see Akhmanova and Steinmetz, 2008). It has been proposed that dimerization is an essential feature required for the plus-end tracking behavior of the EBs and other +TIPs (Slep and Vale, 2007). EBs terminate with a flexible acidic tail containing the C-terminal EEY/F sequence, which is important for self-inhibition and binding to various partners (Hayashi et al., 2005; Akhmanova and Steinmetz, 2008). Through their C-terminal sequences, EBs interact with most other known

Y. Komarova, C.O. De Groot, and I. Grigoriev contributed equally to this paper.

Correspondence to Anna Akhmanova: a.akhmanova@erasmusmc.nl

Y. Komarova's present address is Department of Pharmacology, University of Illinois College of Medicine, Chicago, IL 60612.

J.M. Schober's present address is Southern Illinois University School of Pharmacy, Edwardsville, IL 62026.

S. Honnappa's present address is Novartis Pharma AG, CH-4000 Basel, Switzerland.

G.G. Borisy's present address is Marine Biological Laboratory, 7MBL Street, Woods Hole, MA 02543.

Abbreviations used in this paper: CH, calponin homology; DIC, differential interference contrast; EB, end binding protein; HA, hemagglutinin; IP, immunoprecipitation; MT, microtubule; +TIPs, microtubule plus-end tracking proteins; TIRFM, total internal reflection fluorescence microscopy.

The Rockefeller University Press $30.00
J. Cell Biol. Vol. 184 No. 5 691–706
www.jcb.org/cgi/doi/10.1083/jcb.200807179

Supplemental Material can be found at:
http://jcb.rupress.org/cgi/content/full/jcb.200807179/DC1

Published March 2, 2009

+TIPs and recruit many of them to the growing MT ends (Akhmanova and Steinmetz, 2008).

Recently, the plus-end tracking phenomenon has been reconstituted in vitro using purified +TIPs from fission yeast (Bieling et al., 2007) and vertebrates (Bieling et al., 2008; Dixit et al., 2009). EB1 and its yeast homologue, Mal3, were able to accumulate at the growing MT ends on their own, in the absence of other factors. Moreover, EB1 and Mal3 were required for the plus-end tracking behavior of other +TIPs, confirming the idea that EBs form the core of plus-end tracking complexes. Measurements of EB protein dynamics showed that they exchange very rapidly at the growing MT ends (Busch and Brunner, 2004; Bieling et al., 2007, 2008; Dragestein et al., 2008; Dixit et al., 2009), suggesting that they recognize some specific structural feature associated with MT polymerization.

Inactivation of EBs has profound effects on MT organization and dynamics. EBs are involved in MT anchoring at the centrosome (Rehberg and Graf, 2002; Louie et al., 2004; Yan et al., 2006) and cilia formation (Schroder et al., 2007). The effects of the EBs on MT plus-end dynamics vary between different experimental systems. In budding yeast and in cultured *Drosophila* cells EB1 homologues make MTs more dynamic and decrease the time MTs spend pausing (Tirnauer et al., 1999; Rogers et al., 2002; Wolyniak et al., 2006). In *Xenopus* extracts EB1 stimulates MT polymerization, promotes MT rescues, and inhibits catastrophes (Tirnauer et al., 2002). Also, the fission yeast homologue of EB1 inhibits catastrophes and stimulates the initiation of MT growth (Busch and Brunner, 2004). However, when reconstituted with purified tubulin, both EB1 and Mal3 appeared to stimulate not only rescues but also catastrophes, suggesting that they alter MT end structure, possibly by increasing the size of tubulin sheets (Bieling et al., 2007; Vitre et al., 2008). It should be noted that another study on in vitro reconstitution of MT dynamics with purified tubulin did detect catastrophe suppression by EB1 (Manna et al., 2007), while yet another study observed no effect of EB1 (Dixit et al., 2009). Structural studies suggest that the EBs probably act by enhancing lateral interactions between individual protofilaments and may affect MT lattice structure (Sandblad et al., 2006; des Georges et al., 2008; Vitre et al., 2008).

Despite these significant advances, important questions remain unanswered. Does the in vivo modulation of MT dynamics by EBs depend on their interactions with their numerous partners? Is MT tip association of the EBs sufficient to affect MT dynamics? Is dimerization important for different aspects of EB function? Do all EBs act in the same way? The latter question is particularly important for mammalian cells, which express three members of the EB family—EB1, EB2 (RP1), and EB3 (EBF3) (Juwana et al., 1999; Su and Qi, 2001; Komarova et al., 2005). So far, functional analyses have been mostly focused on EB1: depletion of EB1 in mouse fibroblasts promoted MT pausing and decreased the time MT spent in growth (Kita et al., 2006). Another study demonstrated the involvement of EB1 in formation of stable MTs (Wen et al., 2004). The other two EBs, EB2 and EB3, remained largely ignored, although analysis in differentiating muscle cells did point to a specific function of EB3 (Straube and Merdes, 2007).

Here we show that MT catastrophe suppression is the major activity of mammalian EBs in cultured cells; EB2 is much less potent compared with EB1 and EB3. This functional difference is, at least in part, due to substitutions in the CH domain. Furthermore, we show that the EBs can heterodimerize through their C-terminal part; we use this property to generate a dominant-negative mutant to confirm the results of protein depletion experiments. Finally, we demonstrate that MT plus-end tracking, dimerization, and partner binding activities of the EBs can be separated; we make use of this finding to dissect the EB domains required for catastrophe inhibition.

Results

Mammalian EBs compete with each other for MT tip accumulation

To address the common and distinct functions of mammalian EBs we determined how they affect the distribution of each other. We used our previously developed short hairpin (sh) RNA-expressing vectors to deplete EB1, EB2, and EB3 in CHO-K1 cells (Komarova et al., 2005). In control CHO-K1 cells EB1 and EB3 antibodies stained ~2 µm-long comet-like structures with a peak of intensity near the MT ends (Fig. 1 A, a). In contrast, EB2 was distributed more evenly over the MT lattice and showed only a very slight accumulation at the tip (Fig.1 A, a). This was not due to competition between EB antibodies because the same result was observed when EB2 alone was stained (Fig. S1 B, available at http://www.jcb.org/cgi/content/full/jcb.200807179/DC1). Depletion of EB1 had no effect on EB3 localization; however, it led to redistribution of EB2 to the outmost MT ends (Fig. 1 A, a′). Depletion of either EB2 or EB3 had no effect on the distribution of the remaining EBs (Fig. 1, B and C, b, c). Simultaneous depletion of EB1 and EB3 caused a redistribution of EB2 similar to that induced by the depletion of EB1 alone (Fig. 1 D, d). These observations demonstrate that the EBs accumulate at MT tips independently of each other and suggest that EB2 might be competed by EB1 and EB3 from the outmost MT tips. EB1 appears to be expressed in CHO-K1 cells at higher levels than EB3 (unpublished data), which probably explains why the single depletion of EB1, but not EB3, had an effect on EB2 localization.

Simultaneous depletion of EB1 and EB3 increases MT catastrophe frequency in the internal cytoplasm

We examined the roles of EBs in controlling MT dynamics by expressing YFP-tagged +TIP CLIP-170 to visualize MT growth or by microinjecting cells with Cy3-labeled tubulin. To achieve highly efficient and uniform protein depletion, shRNA vectors were introduced into cells by nuclear microinjection. In control cells, MTs grew persistently from the centrosome to the cell margin where they underwent frequent transitions between growth and shortening, and the distribution of the growing plus-ends along the cell radius was steeply ascending, in agreement with previously published data (Fig. 2 , A and C–E, Table I) (Komarova et al., 2002b). Depletion of single EB species had no effect on persistent MT growth (Table I; unpublished data for

Published March 2, 2009

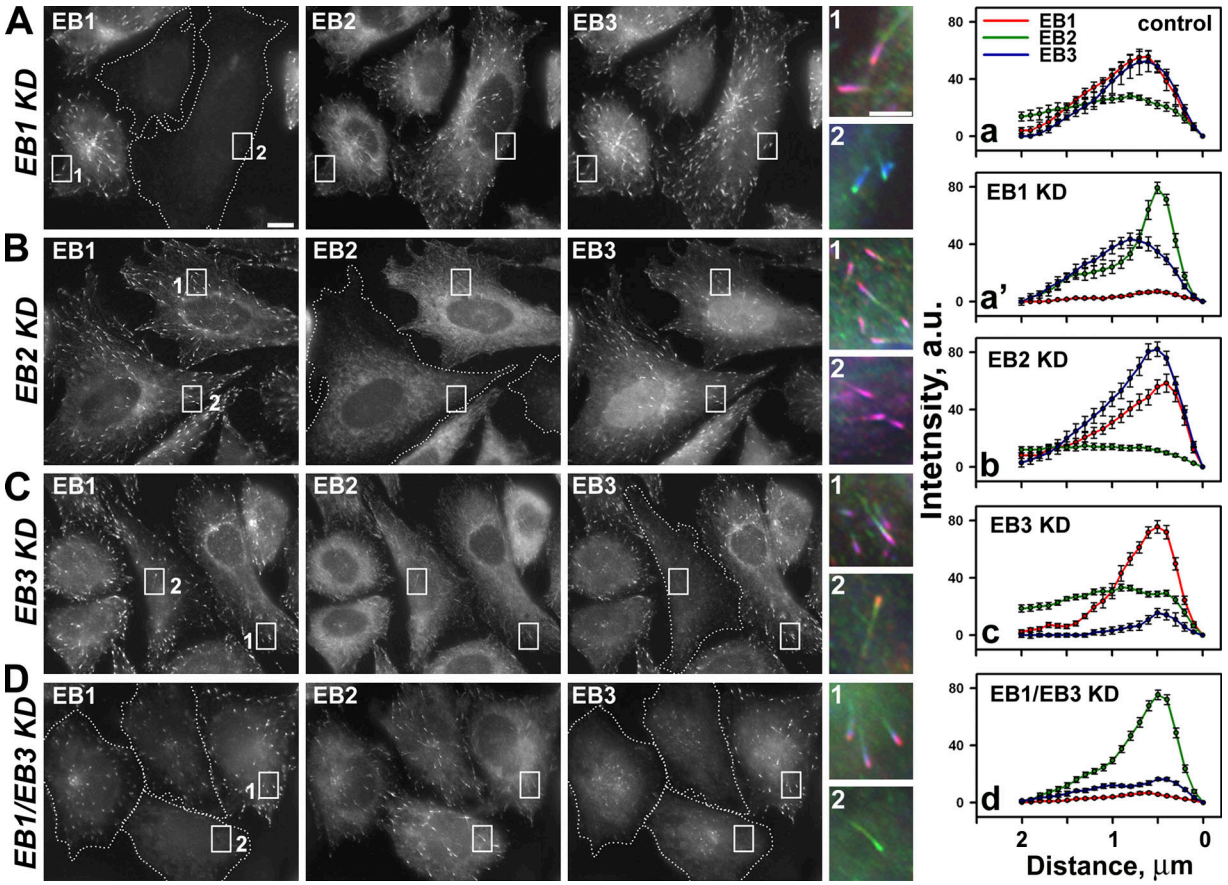

Figure 1. **Effects of depletion of individual EBs on the distribution of other EB1 family members.** (A–D) Immunofluorescent staining of the CHO-K1 cells for EB1, EB2, and EB3 after knocking down EB1 (A); EB2 (B); EB3 (C); or EB1 and EB3 simultaneously (D). EB-depleted cells are indicated by dotted lines. Bar, 10 μm. Enlarged insets from control (1) and EB-depleted cells (2) are shown in color; EB1 is red, EB2 is green, and EB3 is blue in the overlays. Bar, 5 μm. Averaged intensity distributions for each EB protein (±SEM) were obtained for 15–25 MT ends per condition; the values obtained in control cells from each experiment were used for normalization. Intensity distributions are shown for a control cell (a) and for cells depleted of EB1 (a′), EB2 (b), EB3 (c), or EB1 and EB3 simultaneously (d).

EB2 and EB3 depletion). Next, we attempted to deplete all EBs but found that complete knockdown of all three EBs was incompatible with cell viability (unpublished data). However, EB1 and EB3 could be efficiently depleted simultaneously: 3 d after shRNA microinjection the accumulation of EB1 and EB3 at the MT tips was uniformly diminished by ∼90% (Fig. S2 A). In such cells, YFP-CLIP-170 signal at MT tips was diminished as described previously (Komarova et al., 2005; Fig. 2 B), but it could still be used as a reliable marker of growing MT ends, as the parameters of MT growth obtained with YFP-CLIP-170 were very similar to those obtained using subtracted images of Cy3-tubulin (Table I). MT growth rate remained unchanged in these conditions; however, the length of microtubule growth episodes was decreased by a factor of 2 and only 30% of MT ends were concentrated near the cell margin (Fig. 2, C–E and Videos 1 and 2, available at http://www.jcb.org/cgi/content/full/jcb.200807179/DC1; and Table I). Furthermore, MTs underwent catastrophe events in internal cell regions and not just at the cell margin; the catastrophe frequency increased 10-fold (Table I). MT growth phases were often interrupted by pauses followed by shortening (Fig. S2, C and D; Videos 1 and 2). By contrast, MTs in control cells showed hardly any pauses in internal cytoplasm (Fig. S2, B and D; Videos 1 and 2; Table II). Other parameters of MT plus-end dynamics were not significantly affected (Table II); for instance, MT rescue frequency remained unchanged. These data indicate that EB1 and EB3 are not required for MT rescue in CHO-K1 cells.

The acidic tail of EB1 required for partner binding is not needed for catastrophe suppression

To support the specificity of our shRNA-based assays we performed rescue experiments with EB1 constructs insensitive to shRNA (Komarova et al., 2005). We co-microinjected the cells with a plasmid encoding YFP-CLIP-170 together with a vector co-expressing shRNAs against EB1 and EB3 and a rescue construct encoding either the full-length EB1 or EB1ΔAc (an EB1 deletion mutant lacking the last 18 amino acids). For the full-length EB1 it was impossible to assess the efficiency of substitution of the endogenous proteins with the rescue construct; this was, however, possible for EB1ΔAc by using the tail-specific EB1 antibody KT51, which does not react with EB1ΔAc but does detect the endogenous EB1 (Komarova et al., 2005). By combining it with the antibodies that detect total EB1 and EB3 pools, we could show that in cells co-microinjected with the EB1/EB3 shRNA vector and the EB1ΔAc mutant, the levels of

Published March 2, 2009

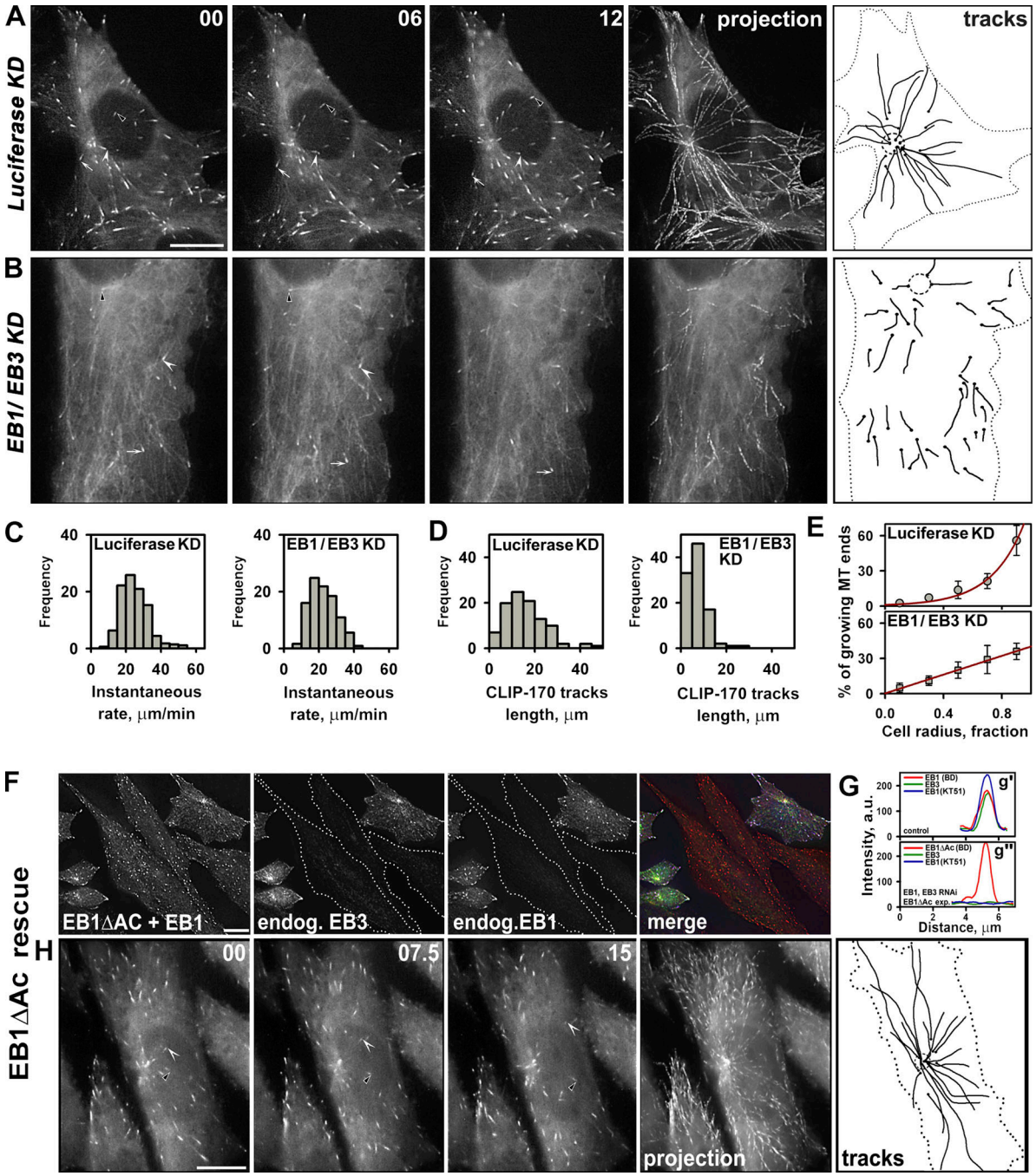

Figure 2. **Simultaneous depletion of EB1 and EB3 disrupts persistent MT growth.** (A and B) Time-lapse sequence of YFP-CLIP-170 in cells expressing shRNAs either to luciferase (control) (A) or to EB1 and EB3 (B). Images were acquired every 2 s. Three tips of CLIP-170 "comets" are indicated by an arrow, an arrowhead, and a black-and-white arrowhead. Projection analysis (20 successive frames) and diagrams of trajectories of individual CLIP-170 comets illustrate episodes of uninterrupted MT growth. The centrosome region is indicated by a dashed circle; the cell border is shown by a dotted line. Time in seconds is in the top right corner. Bar, 10 μm. (C and D) Histograms of MT growth rates and the lengths of YFP-CLIP-170 tracks in control (luciferase) and EB1/EB3 shRNA-expressing cells. (E) Distribution of the growing MT plus-ends along the cell radius in control and EB1/EB3-depleted cells; error bars indicate SD. The cell radius was divided into five zones (each zone was a 0.2 fraction of the cell radius) and the number of YFP-CLIP-170–positive tips were scored for each zone (~600 MT tips in 8–12 cells for each condition). The results are represented as percentage of the MTs within each zone where 100% is a total number of the scored growing plus-ends in the cell. (F and G) Rescue of EB1/EB3 depletion by EB1ΔAc. (F) EB1/EB3-depleted cells expressing EB1ΔAc are indicated by dotted lines. EB3 was detected with rabbit antibodies (green in overlay); EB1 was stained with the mouse antibody from BD Biosciences, which detects both the endogenous EB1 and EB1ΔAc (left panel; red in overlay); and the rat antibody KT51 (Absea), specific for the acidic tail of EB1, was used to stain the endogenous EB1 but not EB1ΔAc (right panel; blue in overlay). (G) Intensity distribution shows that the levels of endogenous EB1 and EB3 in EB1ΔAc-rescued cells were negligible (green and blue lines in panel g′′); level of EB1ΔAc (red line in panel g′′) was similar to the level of endogenous EB1 (red line in panel g′). (H) Time-lapse sequence of YFP-CLIP-170 in the cells coexpressing shRNAs to EB1/EB3 and EB1ΔAc rescue construct; images were acquired every 2.5 s. Tips of CLIP-170 comets are indicated by white and black-and-white arrowheads. Projection analysis and trajectories of individual YFP-CLIP-170 comets are generated in the same way as in panel A. Time in seconds is in the top right corner. Bar, 10 μm.

Published March 2, 2009

Table I. **Parameters of MT growth in CHO-K1 cells**

	Number of observations	Length of uninterrupted growth[a]	Growth rate[b]	Catastrophe frequency[c]
		μm	$\mu m/min$	min^{-1}
Expression of shRNA				
Luciferase; YFP-CLIP-170	100 MTs; 7 cells	15.6 ± 8.8	24.3 ± 8.3	0.3 ± 0.1
Luciferase; Cy3-tubulin	37 MTs; 3 cells	13.4 ± 5.9	18.5 ± 5.3	0.2 ± 0.1
EB1; YFP-CLIP-170	88 MTs; 7 cells	14.5 ± 6.4	21.4 ± 9.4	0.3 ± 0.1
EB1/EB3; YFP-CLIP-170	101 MTs; 8 cells	7.3 ± 4.5	22.6 ± 8.4	3.2 ± 0.9
EB1/EB3; Cy3-tubulin	56 MTs; 3 cells	7.4 ± 4.1	22.4 ± 5.5	3.7 ± 0.7
Rescue experiments in EB1/EB3-depleted cells				
EB1 rescue; YFP-CLIP-170	64 MTs; 7 cells	15.1 ± 7.0	21.1 ± 8.0	0.3 ± 0.1
EB1ΔAc rescue; YFP-CLIP-170	96 MTs; 10 cells	16.6 ± 7.3	26.9 ± 10.7	0.3 ± 0.1
Expression of EB1 mutants				
EB1-NL (control); YFP-CLIP-170	88 MTs; 7 cells	18.5 ± 7.1	22.5 ± 7.1	0.2 ± 0.1
EB1-CΔAc; YFP-CLIP-170	116 MTs; 9 cells	4.5 ± 2.9	20.3 ± 7.9	4.2 ± 1.0
EB1-CΔAc; Cy3-tubulin	55 MTs; 4 cells	4.8 ± 3.4	18.7 ± 7.8	3.5 ± 0.9

[a]The length of YFP-CLIP-170 or tubulin tracks represents the length of persistent growth.
[b]The growth rate ± SD was calculated from the histogram of displacements of YFP-CLIP-170–positive tips or Cy3-labeled MT ends between successive frames.
[c]The catastrophe frequency (the number of transition events over time) was calculated for each cell and was presented as an average ± SD for the cell population.

residual endogenous EB1 and EB3 proteins were negligible while the expression of the EB1ΔAc mutant was comparable to the level of endogenous EB1 in control cells (Fig. 2, F and G). Both EB1 and EB1ΔAc expression fully restored persistent MT growth in EB1/EB3-depleted cells (Fig. 2 H; Table I). Moreover, we observed no difference in catastrophe frequency after the expression of either full-length EB1 or the EB1ΔAc mutant (Table I). This suggests that EB1 might control persistent MT growth independently of its interaction with the CLIPs, dynactin, CLASPs, APC, and other partners that bind to the EBs in a tail-dependent fashion (Hayashi et al., 2005; Honnappa et al., 2005; Komarova et al., 2005; Mimori-Kiyosue et al., 2005; Weisbrich et al., 2007).

EB1 dimerization domain acts as a dominant-negative mutant

Because we could not achieve a complete knockdown of all EB species, we sought to design a dominant-negative mutant that could be used to remove the three EB family members from MT plus-ends. EBs dimerize through a thermodynamically stable coiled-coil domain in the C-terminal part of the protein (Honnappa et al., 2005; Slep et al., 2005) (Fig. 3 A). We first investigated

Table II. **Parameters of MT shortening in CHO-K1 cells**

	At the cell periphery				In internal cytoplasm			
	Number of observations	[a]Rate of shortening	[b]Rescue frequency	[c]Length of shortening	Number of observations	[a]Rate of shortening	[b]Rescue frequency	[c]Length of shortening
		$\mu m/min$	min^{-1}	μm		$\mu m/min$	min^{-1}	μm
Control cells	200 MTs; 10 cells	30.0 ± 9.4	10.0 ± 1.8	2.9 ± 3.4	N/A	N/A	N/A	N/A
EB1/EB3 depleted cells	118 MTs; 6 cells	23.4 ± 10.8	10.0 ± 1.5	2.4 ± 2.5	58 MTs; 7 cells	29.6 ± 11	8.1 ± 1.8	3.45 ± 2.4
EB1-CΔAc	102 MTs; 5 cells	23.7 ± 8.6	7.8 ± 2.0	2.9 ± 2.3	75 MTs; 5 cells	23.2 ± 8.8	6.7 ± 2.0	4.3 ± 3.0

N/A, not applicable. The analysis was precluded by extremely low catastrophe frequency in internal cell regions.
[a]The shortening rate ± SD was calculated from the histogram of displacements of shortening MT tips between successive frames using subtracted images.
[b]The rescue frequency (the number of transition events over time) was calculated for each cell and was presented as an average ± SD for the cell population.
[c]The length of uninterrupted shortening.

Published March 2, 2009

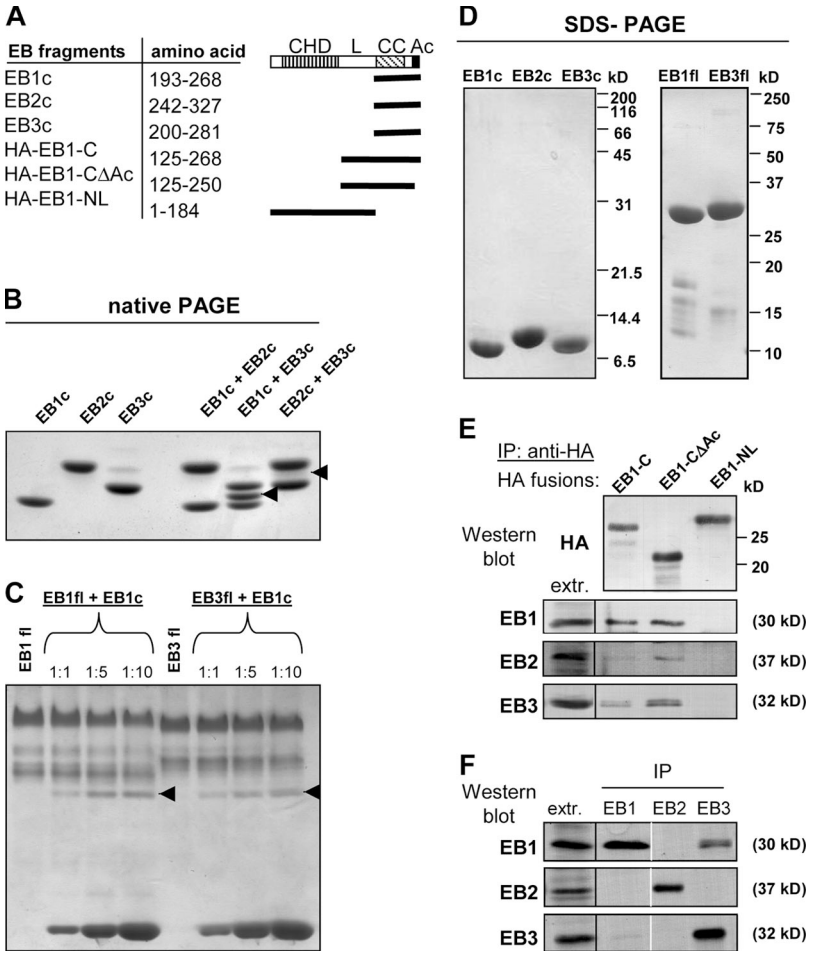

Figure 3. **The C-terminal domain of EB1 heterodimerizes with the full-length EBs.** (A) Schematic representation of EB constructs used for the heterodimerization and co-IP assays. CHD, calponin homology domain; L, linker; CC, coiled coil; Ac, acidic tail. (B and C) Analysis of the indicated proteins or protein mixtures by native 15% (B) or 9% (C) PAGE at 4°C. EBc fragments were mixed in an equimolar ratio (B); EB1c and the full-length EB1 and EB3 were mixed in different ratios as indicated (C). Heterodimers are indicated by arrowheads. (D) Analysis of the indicated proteins by denaturing SDS-PAGE; molecular weight markers are indicated on the right. (E) Co-IPs of HA-tagged EB1 mutants expressed in COS-1 with an HA antibody. Western blots were probed with the indicated antibodies. EB1-C and EB1-CΔAc but not EB1-NL co-precipitate the endogenous EBs. Extr. = 10% of the cell extract, used for IP. (F) Co-IPs of endogenous EBs from COS-1 cells. Extr. = 10% of the cell extract, used for IP.

whether the EB dimerization domains are kinetically stable by mixing purified C-terminal fragments of EB1, EB2, and EB3 (EB1/2/3c) in various combinations at 37°C and analyzing the mixtures by native PAGE at 4°C. We observed significant and spontaneous heterodimer formation between EB1c and EB3c but only very little or no dimerization with EB2c (Fig. 3 B, arrowheads). This result suggests that EBs can potentially heterodimerize. We next investigated if the C-terminal domain of EB1 can disrupt the full-length EB1 and EB3 dimers, and indeed observed heterodimer formation (Fig. 3 C, arrowheads). Similar results were obtained when EB3c was mixed with full-length EB1 and EB3 (unpublished data). All analyzed proteins looked homogenous on denaturing and reducing gels (Fig. 3 D), indicating that the appearance of additional bands on the native gels resulted from heterodimerization.

Next, we used co-immunoprecipitation (co-IP) to investigate whether heterodimerization can also occur in cells. The C-terminal EB1 fragments EB1-C and EB1-CΔAc (which lacks the acidic tail, Fig. 3 A), but not the N-terminal portion of EB1 (EB1-NL, lacking the coiled-coil domain and the C terminus, Fig. 3 A) coimmunoprecipitated all three EB family members (Fig. 3 E). It is unclear why the interaction between the dimerization domains of EB1 and EB2 was inefficient in vitro but did occur in cells; it could be influenced by temperature and buffer conditions, posttranslational modifications, additional cellular factors, and/or the presence of the linker region in EB1-C and EB1-CΔAc.

Finally, we investigated if endogenous EBs heterodimerize. Using antibodies specific for the three EB species, we found no heterodimer formation with EB2, but a significant co-IP of endogenous EB1 and EB3 (Fig. 3 F). This result was not due to cross-reactivity of the used EB3 antibody with EB1 because we observed no co-IP of EB1 with the EB3 antibody from HeLa cells, where EB3 is expressed only at very low levels and is not immunoprecipitated efficiently (unpublished data). A weak co-IP of EB3 with EB1 was also observed; the differences in efficiency of the co-IP of EB1-EB3 dimers with EB1 and EB3 antibodies is most likely caused by the fact that EB1 is expressed at higher levels than EB3 in CHO-K1 cells (unpublished data), and its relative proportion tied up in heterodimers is lower. Based on these data we conclude that EB1 and EB3 can form heterodimers in cells.

Formation of a heterodimer between a full-length EB molecule and the C-terminal fragment will produce a protein that would have only one MT-binding domain and a reduced affinity for MTs (see below). In line with this idea, overexpression of EB1-C and EB1-CΔAc had a profound effect on the distribution of all EB family members, whereas the overexpression of EB1-NL had no consequences for the endogenous EB distribution (Fig. S1, and unpublished data). Quantification

Published March 2, 2009

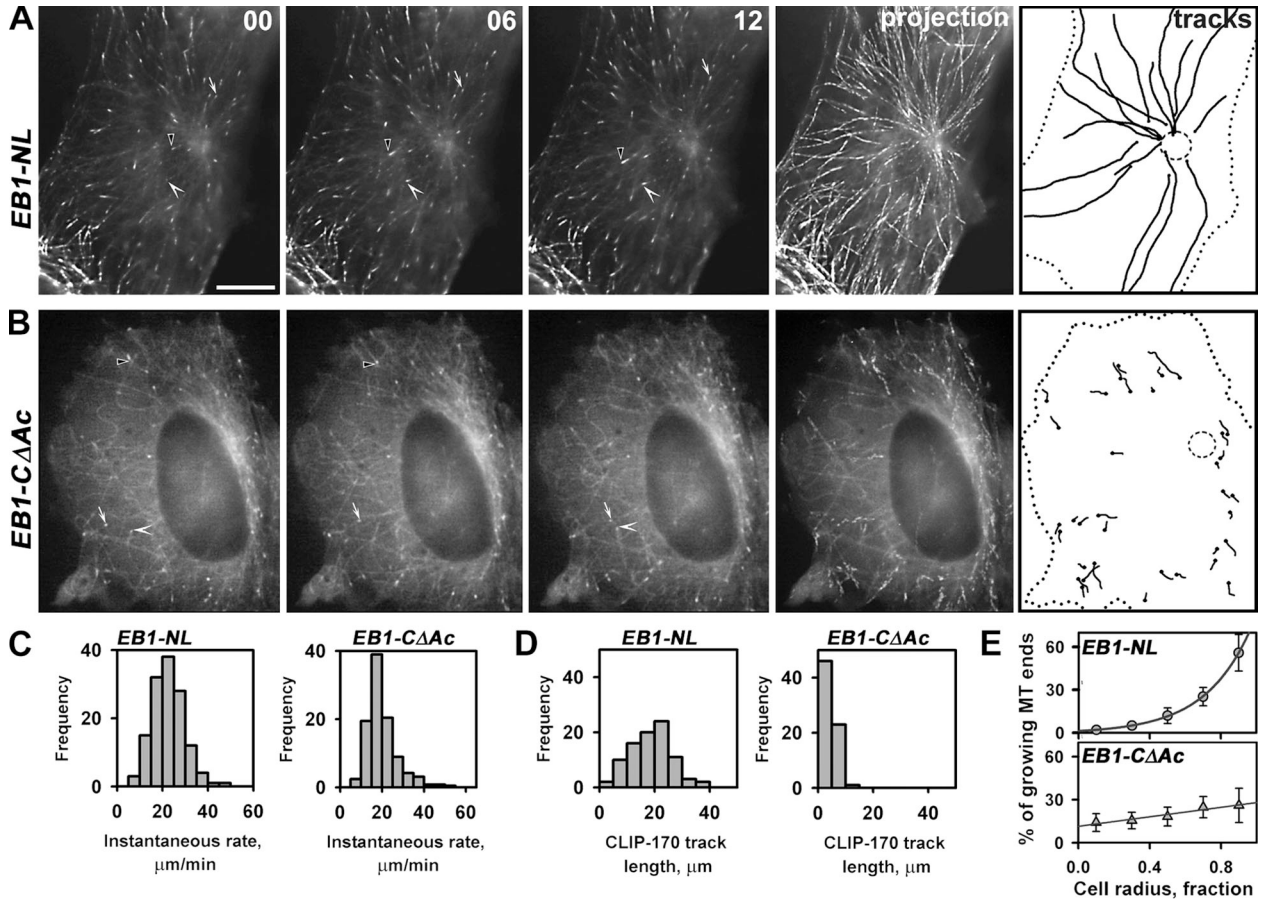

Figure 4. **Expression of the dominant-negative EB1 mutant disrupts persistent MT growth in CHO-K1 cells.** (A and B) Representative time-lapse images of YFP-CLIP-170 in cells expressing HA-EB1-NL (control) and HA-EB1-CΔAc (dominant negative) mutants. Images were acquired every 2 s. Tips of three YFP-CLIP-170 comets are indicated over time by an arrow, an arrowhead, and a black-and-white arrowhead. Projection analysis and trajectories of individual YFP-CLIP-170 comets are generated in the same way as in Fig. 2 A. Time in seconds is shown in the top right corner. Bar, 10 μm. (C and D) Histograms of the instantaneous MT growth rates and the lengths of YFP-CLIP-170 tracks in HA-EB1-NL and HA-EB1-CΔAc-expressing cells. (E) Distributions of the growing MT plus-ends along the cell radius in EB1-NL and EB1-CΔAc–expressing cells presented as in Fig. 2 E; error bars represent SD.

of the EB signals demonstrated that only 21 ± 6%, 27 ± 10%, and 13 ± 5% (average ± SD) of EB1, EB2, and EB3, respectively, remained at MT ends in cells expressing the EB1-CΔAc mutant. We conclude that C-terminal fragments of EB1 act in a dominant-negative fashion, reducing the accumulation of all three EBs at MT tips.

Overexpression of the dominant-negative EB1 fragment increases catastrophe frequency

We next analyzed the effect of EB1-CΔAc expression on MT dynamics. This EB1 fragment is deficient in binding to CLIPs, $p150^{Glued}$, CLASPs, APC, and MCAK and is therefore not expected to directly influence these +TIPs (Hayashi et al., 2005; Honnappa et al., 2005; Komarova et al., 2005; Mimori-Kiyosue et al., 2005; Weisbrich et al., 2007; unpublished data). MT growth was analyzed using Cy3-labeled tubulin or YFP-CLIP-170 in cells overexpressing either EB1-CΔAc or EB1-NL (Fig. 4, A and B; Table I). The latter protein, when overexpressed at high levels, bound weakly along the whole MT lattice and its overexpression did not affect the growth rate or MT growth persistency (Fig. 4, A, C, and D; Table I). The mean length of uninterrupted MT growth was similar to that in control cells (Table I) and the distribution of the growing plus-ends along the cell radius was steeply ascending (Fig. 4 E). In contrast, the overexpression of the EB1-CΔAc severely reduced the length of MT growth episodes (Fig. 4, B and D). Although the rate of MT growth (Fig. 4 C) or parameters of MT shortening (Table II) did not significantly change, the catastrophe frequency was increased similarly to the effect of EB1/EB3 depletion (Table I). MT dynamics alteration led to a dramatic reduction in the proportion of growing plus-ends at the cell periphery (Fig. 4 E). We conclude that mammalian EB1 family members ensure persistent MT growth in cells.

Monomeric EB3 mutant tracks growing MT ends in cells and in vitro

The dominant-negative EB1 mutant strongly suppressed anti-catastrophe activity of endogenous EBs without causing their complete depletion from MT tips (Fig. S1). A possible explanation of this result is that the heterodimeric proteins containing one MT-binding domain are still able to bind, albeit weakly, to MT ends. Indeed, while by themselves GFP-tagged EB1-C or EB1-CΔAc were diffusely distributed in

Published March 2, 2009

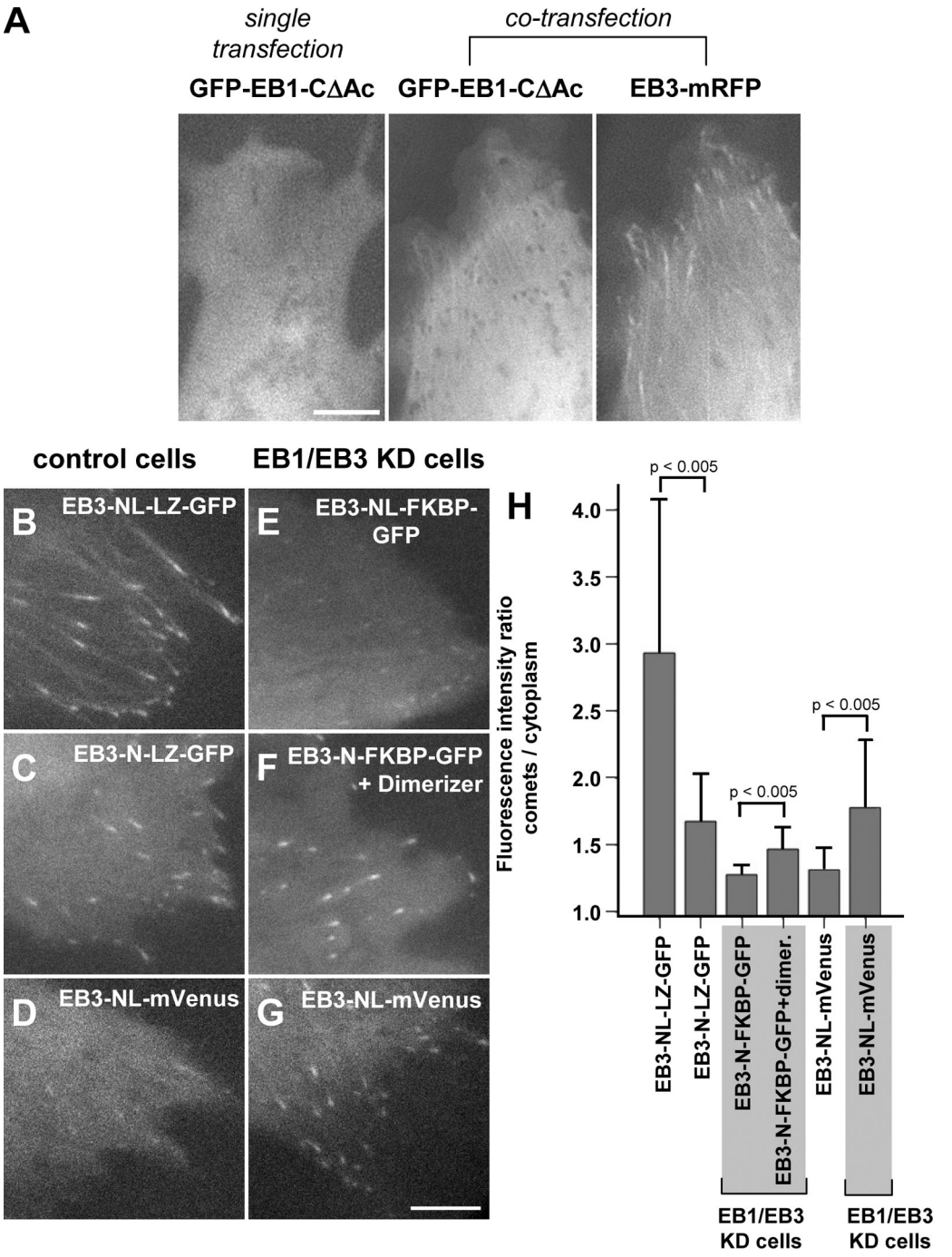

Figure 5. **Monomeric N terminus of EB3 tracks growing MT ends in cells.** (A) Live images of CHO-K1 cells transfected with GFP-EB1-CΔAc alone or together with EB3-mRFP. Images were processed by applying Blur filter and Unsharp Mask in Photoshop. Bar, 5 µm. (B–G) Live images of control CHO-K1 cells (B–D) or EB1/EB3-depleted cells (E–G) expressing the indicated constructs. Cells expressing similar low levels of the fusion proteins were selected based on average fluorescence intensity. Bar, 5 µm. (H) Ratio of fluorescence intensities at the growing MT tips and in surrounding cytoplasm (after background subtraction), measured from live cell images obtained as described for panels B–G. 10 cells (45–200 MT tips) were measured for each construct; error bars represent SD. The differences between the indicated values were significantly different; statistical analysis was performed using nonparametric Mann-Whitney *U* test.

the cytoplasm, these proteins were weakly recruited to the distal MT stretches when a full-length EB3 tagged with mRFP was overexpressed in the same cells (Fig. 5 A and unpublished data).

A previous study showed that the N-terminal part of EB1 fused to a regulated dimerization domain was unable to bind to MT tips in the absence of dimerizer and was strongly bound to MT ends after dimerizer addition (Slep and Vale, 2007). This result was interpreted as an indication that dimerization is essential for the plus-end tracking behavior. An alternative explanation is that monomeric CH domain-containing EB fragments do not efficiently compete with endogenous EBs for MT tips

Published March 2, 2009

and therefore their accumulation at MT ends is low. If this assumption were correct, the binding of monomeric CH domain–containing EB fragments to MT tips should improve in the absence of endogenous EBs. To test this idea, we first confirmed that the EB3 N-terminal portion, artificially dimerized by the addition of the leucine zipper (LZ) domain of GCN4 (EB3-NL-LZ), efficiently accumulated at MT tips, indicating that the coiled-coil domain and the acidic tail of EB3 are not needed for plus-end tracking (Fig. 5, B and H; see Fig.7 for a scheme of the fusions). An artificial dimer of the EB3 CH domain lacking most of the linker region (EB3-N-LZ) also tracked plus-ends, albeit less efficiently (Fig. 5, C and H), indicating that the linker region of the EBs contributes to MT binding but is not essential. Next, we fused EB3-N to the homodimerization domain FKBP; as a monomer, it showed hardly any plus-end tracking in control cells (unpublished data) but displayed MT end accumulation, albeit weak, in cells depleted of EB1 and EB3 (Fig. 5 E). Plus-end accumulation of this protein was enhanced by dimerizer addition (Fig. 5, F and H), indicating that the monomeric version of the construct can still plus-end track, but dimerization enhances its binding to MT tips.

To exclude potential weak dimerization of EB3-N through FKBP or GFP, we next tested whether EB3-N or EB3-NL fused to a monomeric version of the fluorescent protein Venus (mVenus) can bind MT tips. EB3-NL-mVenus displayed clear plus-end tracking in EB1/EB3 knockdown cells but only a weak plus-end binding in control cells (Fig. 5, D, G, and H). EB3-N-mVenus showed no plus-end accumulation (unpublished data), indicating that the linker region contributes to MT binding, in line with the recently published data on Mal3 (des Georges et al., 2008).

To investigate the oligomerization state of EB3-NL-mVenus, we fused it to a 6xHIS tag and purified it from bacteria. Size-exclusion chromatography and static light scattering (SLS) analysis yielded an average molecular mass of 56.3 kD (Fig. S3 A, available at http://www.jcb.org/cgi/content/full/jcb.200807179/DC1), in agreement with the calculated molecular mass of the protein (51.4 kD). This result shows that EB3-NL-mVenus is indeed a monomer. In contrast, GFP-EB3 displayed an average molecular mass of 128 kD (Fig. S3 A), consistent with the formation of a dimer (calculated molecular mass 127.8 kD).

We next used purified full-length GFP-EB3 and EB3-NL-mVenus fusions to reconstitute plus-end tracking in vitro using the approach described by Bieling et al. (2007). Both the full-length EB3 dimer and the monomeric EB3-NL-mVenus protein weakly decorated the MT lattice and strongly accumulated at the growing plus- and minus-ends; the labeling of the rapidly growing plus-ends was higher than that of slowly growing minus-ends (Fig. 6, A–D; Videos 3 and 4, available at http://www.jcb.org/cgi/content/full/jcb.200807179/DC1). Collectively, our results show that a single CH domain is capable of recognizing growing MT ends in the absence of other +TIPs, and that this process does not rely on dimer formation.

To show that monomeric EB3 binds MT tips less efficiently compared with the dimer, we performed in vitro competition experiments. Increasing levels of purified mCherry-tagged or untagged full-length EB3 were able to suppress the accumulation of EB3-NL-mVenus at the growing MT tips, while its MT lattice binding did not significantly change (Fig. 6, E and F). In contrast, comparable levels of monomeric EB3-NL-mVenus had no effect on the accumulation of mCherry-EB3 at the tips of MTs (Fig. 6, E and F), indicating that the dimeric full-length protein has a higher affinity for the growing MT ends.

Dimerization is required for the anti-catastrophe activity of EB3 in cells

We next set out to test which EB domains are important for MT catastrophe suppression. To be able to screen a broad panel of mutants, we switched to transient cotransfection of shRNA and rescue constructs, which contained a fluorescent tag and therefore could be directly used to detect MT growth (Fig. 7). As a measure of persistent growth, we calculated the percentage of tracks longer than 7.5 µm (approximately half of the cell radius) (Fig. 7). We measured this parameter in control cells by using direct MT labeling with mCherry–α-tubulin and visualizing MT outgrowth from the centrosome within a photobleached cell sector (Fig. S2 E), and by labeling growing MT ends either with GFP-CLIP-170 or EB3-GFP. All three methods produced consistent results and although we used transfection instead of microinjection, MT growth parameters were quite similar to those described above (Fig. 7; Figs. S4 and S5, available at http://www.jcb.org/cgi/content/full/jcb.200807179/DC1). Also under these conditions we observed a strong reduction of persistent MT growth when EB1 and EB3 were depleted, while MT growth rate was not significantly affected (Figs. S4 and S5). In control cells the percentage of tracks longer than 7.5 µm exceeded 80%; it was reduced to ∼40% after simultaneous EB1/EB3 depletion (Fig. 7; Fig. S4). The results obtained with GFP-tagged CLIP-170 and mCherry–α-tubulin were again very similar (Fig. 7). Further, by cotransfecting mCherry–α-tubulin with hemagglutinin (HA)-tagged EB1-CΔAc and monitoring MT growth in photobleached regions, we confirmed the severe disruption of MT growth persistence by this dominant-negative mutant of EB1 (Fig. 7).

Persistent MT growth was completely restored by the expression of the full-length EB3 with a C-terminal GFP tag, or by the GFP-EB3-ΔAc fusion, lacking the acidic tail (Fig. 7; Fig. S4). These results are fully consistent with those obtained with untagged EB1 constructs (Fig. 2 H; Table I), and indicate that the N- or C-terminal GFP tag does not interfere with the catastrophe-suppressing activity of EB3. In contrast, the monomeric protein EB3-NL-mVenus displayed no rescue activity, indicating that accumulation of a single EB3 CH domain at MT ends is by itself insufficient for catastrophe inhibition.

We next tested the artificial EB3 dimers in which the EB3-N or EB3-NL fragments were fused to the GCN4 leucine zipper or FKBP. Interestingly EB3-NL-LZ (but not EB3-N-LZ or the EB3-N-FKBP fusion, with or without dimerizer addition) displayed a significant anti-catastrophe activity: the proportion of long MT growth tracks was increased to ∼75% (Fig. 7; Fig. S4). Because EB3-NL-LZ is completely devoid of any sequences responsible for the binding to the known EB partners, its anti-catastrophe activity is most likely due to its effect on the MT tip. We conclude that in cells anti-catastrophe activity of EB3 requires dimerization of the CH domain and is sensitive to the

Published March 2, 2009

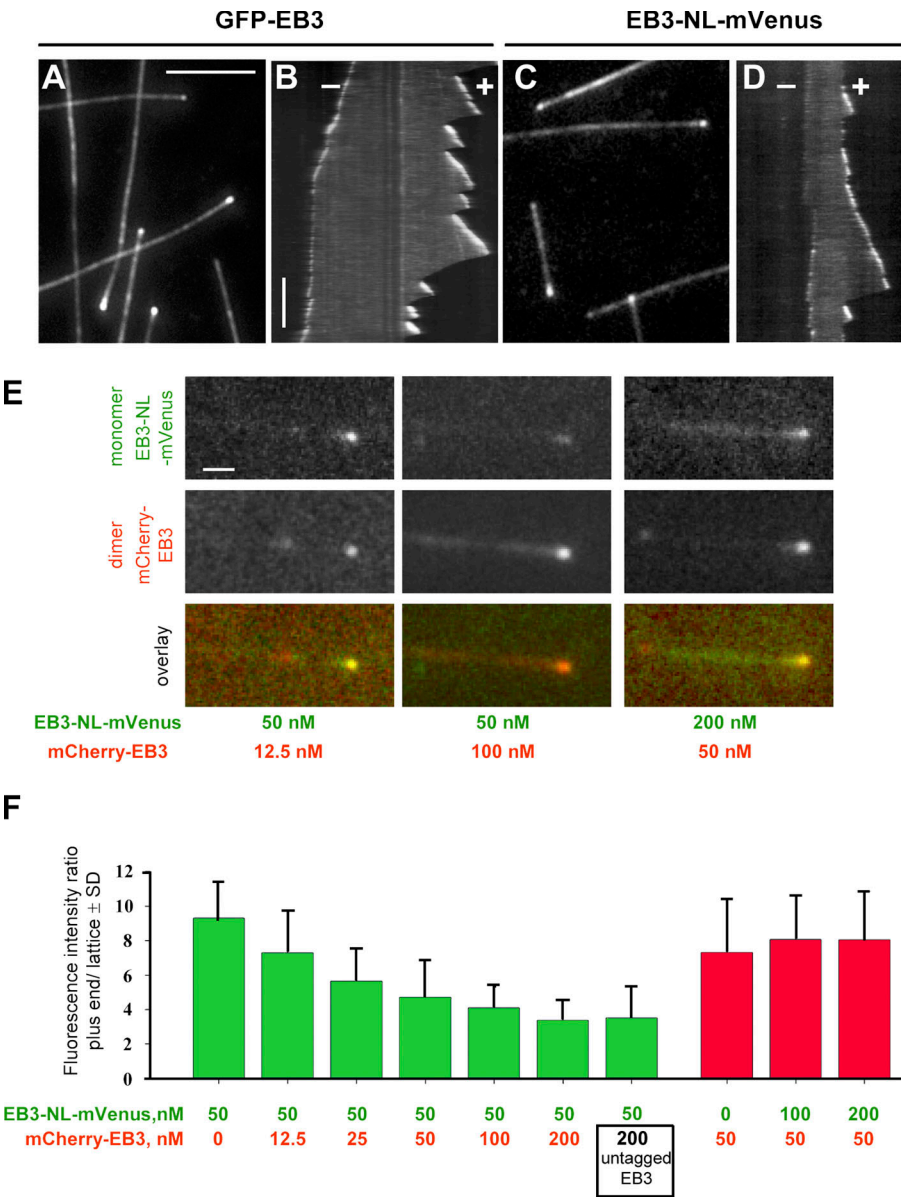

Figure 6. **Monomeric N terminus of EB3 tracks growing MT ends in vitro.** (A–D) In vitro MT plus-end tracking assay. Representative TIRFM images (A and C) and kymographs (B and D) show specific accumulation of GFP-EB3 (100 nM) and EB3-NL-mVenus (100 nM) at the growing, but not shortening MT plus (+) and minus (−) ends. Horizontal bars, 5 µm; vertical bar, 60 s. (E) Dual-color imaging of in vitro plus-end tracking assays performed with the indicated concentrations of EB3-NL-mVenus and mCherry-EB3. Images were processed by applying Blur filter in Photoshop. Bar, 1 µm. (F) Ratio of fluorescence intensity at the growing MT tip and on the MT lattice for the indicated protein mixtures (after background subtraction). Green plots show measurements for EB3-NL-mVenus and red plots for mCherry-EB3. 10–20 MT tips were measured per experiment; error bars represent SD.

adjacent linker sequences, suggesting that the features that increase MT tip association of the EBs are beneficial for catastrophe suppression.

Differences between the N-terminal parts of the EB2 and EB3 CH domains have a large impact on their catastrophe suppression activity

The presence of EB2 alone was insufficient to support processive MT growth (Fig. 2 B); also an overexpression of the GFP-tagged or untagged EB2 could not rescue the effect of EB1/EB3 depletion (Fig. 7; Fig. S4; and unpublished data). EB2 differs from EB1 and EB3 by the presence of an ∼40 amino acid N-terminal extension. We fused this extension to EB3-GFP and found that it had no effect on the capacity of the protein to suppress catastrophes. In contrast, substitution of the first 29 amino acids of EB3 for the corresponding residues of EB2 in the presence or absence of the EB2-specific N-terminal extension significantly compromised the catastrophe-inhibiting activity of EB3 (Fig. 7; Fig. S4).

To get insight into the differences between the CH domains of EB3, EB2, and EB1 (see Fig. 8 A for sequences), we solved the x-ray crystal structure of EB3-CH domain at 1.4 Å resolution (Table S1). The structure of the CH domain of EB3 is very similar to the ones of EB1 (Hayashi and Ikura, 2003; Slep and Vale, 2007) and its yeast orthologue Bim1 (Slep and Vale, 2007; Fig. 8 B). It is formed by seven helices that pack around the central and conserved helix α3. We failed to obtain crystals of EB2-CH; however, because of the high sequence identity between the CH domains of EB1 and EB2 we modeled the EB2-CH structure (see Materials and methods). Using the structures of the CH domains of EB1 and EB3, together with the structural model of EB2 we analyzed and mapped surface residue differences between the three EBs (Fig. 8, C and D). Based on the data from Slep and Vale (2007), we also mapped conserved residues that abrogated MT plus-end tracking of EB1 in cells (Fig. 8, C and D, blue and

Published March 2, 2009

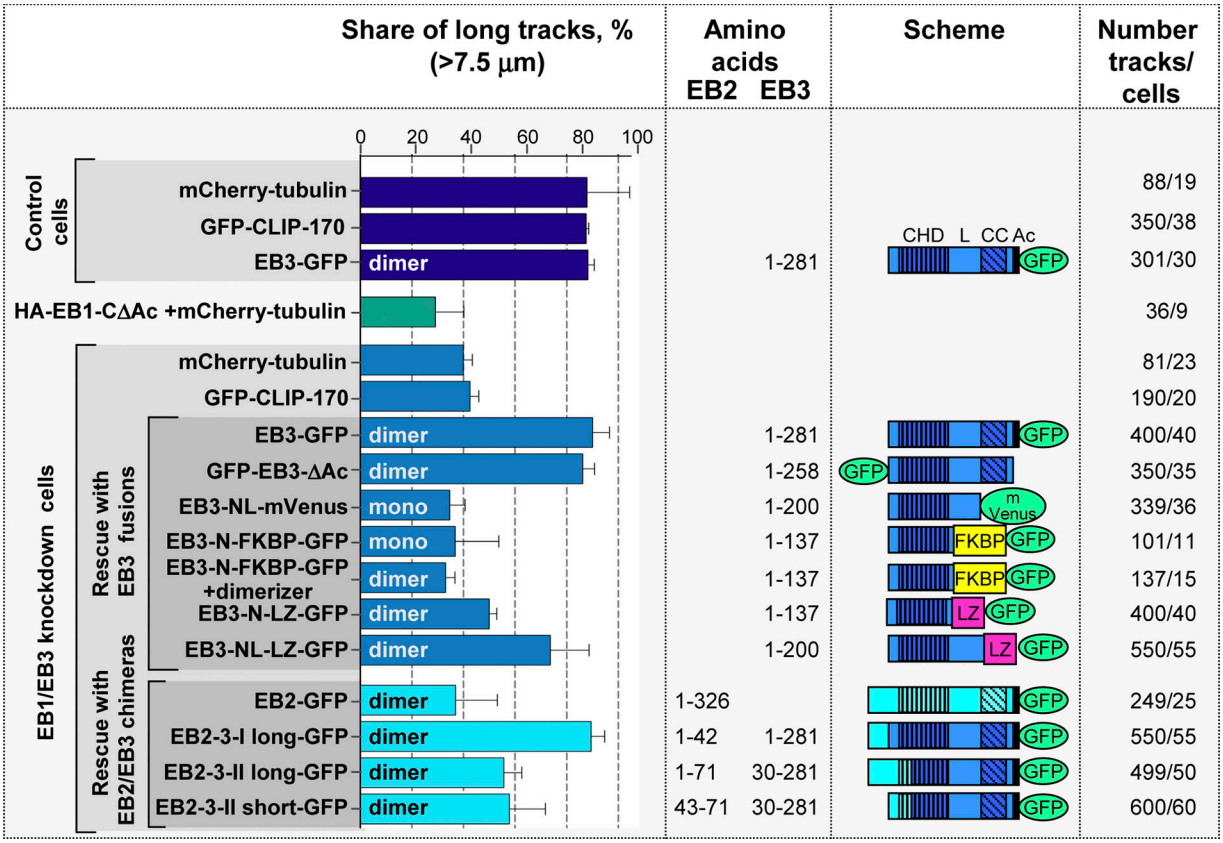

Figure 7. **Rescue of processive MT growth by different EB3 fusions and EB2-EB3 chimeras in EB1/EB3-delpeted cells.** The proportion of MT tracks originating from the centrosome, with the length exceeding 7.5 μm, schematic representations of the constructs, amino acid positions in EB3 and EB2, and the numbers of tracks and cells analyzed for each construct are indicated. Share of long MT growth episodes in control cells, EB1/EB3-depleted cells, and cells expressing HA-EB1-ΔAc obtained using GFP-CLIP-170 or mCherry–α-tubulin (after photobleaching) is shown for comparison. Cells with approximately the same radius were selected for quantification. Error bars indicate SD determined based on 2–4 independent experiments.

purple). Interestingly, most of the residue differences found at the N terminus of EB3-CH domain and EB2-CH domain cluster around a patch of residues formed by the conserved sequence segment 16-SRHD-19, which is critical for MT binding (Fig. 8 C, red). In contrast, differences between EB3 and EB1 are less pronounced: the few residue substitutions are mostly localized in regions that do not affect MT end accumulation (Fig. 8, C and D, green and orange). These findings help to explain why EB3 and EB1 display similar MT binding and catastrophe suppression behaviors, and why EB2 activity is distinct.

EB3 promotes MT catastrophes in vitro

To address whether anti-catastrophe activity is an intrinsic property of EBs, we analyzed the impact of the full-length and monomeric EB3 on MT dynamics reconstituted with purified tubulin in vitro, by imaging MTs with differential interference contrast (DIC) microscopy. The full-length EB3 (with or without the GFP tag) increased MT growth velocity and the frequency of catastrophes and rescues (Fig. S3 B, Table III). This is in line with some previous work on EB1 and Mal3 (Bieling et al., 2007; Vitre et al., 2008), although little effect on MT dynamics in vitro was found in another study (Dixit et al., 2009), and catastrophe suppression by EB1 was described in yet another paper (Manna et al., 2007). These differences are possibly due to use of different tubulin preparations and assay conditions.

Interestingly, the monomeric EB3-NL-mVenus had a very similar, albeit a weaker effect, compared with the full-length protein (Fig. S3 B, Table III), indicating that, at least in conditions used by us in vitro, EB3 does not act through a dimerization-dependent tubulin multimerization, as has been proposed previously (Slep and Vale, 2007). Further, these results show that catastrophe suppression observed in cells is most likely not an intrinsic activity of EB3.

Discussion

The EBs are highly conserved proteins, which can target growing MT tips on their own and are involved in the recruitment of numerous other +TIPs to MT ends, suggesting that they hold the key to understanding the plus-end tracking phenomenon. Using in vitro and in vivo approaches we have shown that a single EB CH domain is necessary and sufficient for specific association with growing MT ends. The linker region, adjacent to the CH domain, as well as the C-terminal dimerization domain, can contribute to MT tip accumulation but are not essential because EB3-N-FKBP and EB3-N-LZ, which lack these domains, still track MT plus-ends. This indicates that a single CH domain is the primary determinant of MT plus-end recognition.

Although dimerization is not required for plus-end tracking, EBs do exist as dimers (Honnappa et al., 2005; Slep et al.,

Published March 2, 2009

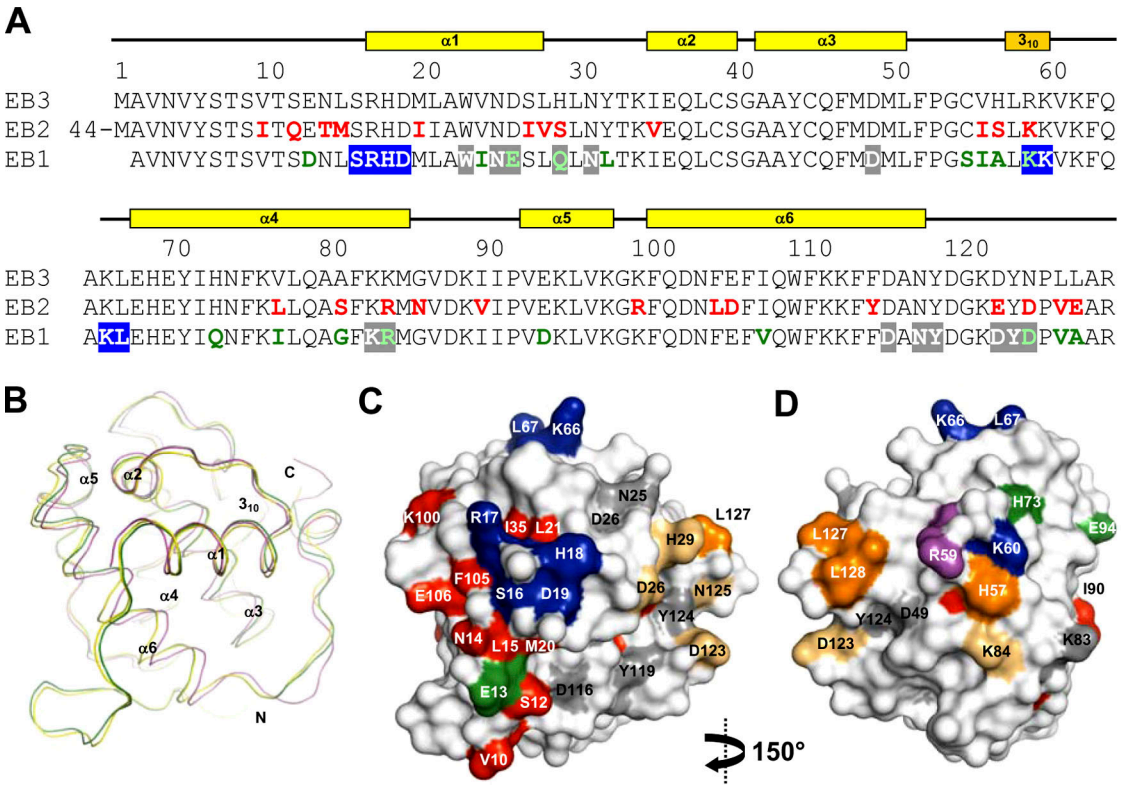

Figure 8. **Structural analysis of EB-CH domains.** (A) Sequence alignment of the three human EB homologues. Residue assignment and secondary structure elements are indicated on the top of the alignment. Residues colored in red and green indicate the differences between EB3 and EB2 (EB2 sequence) and EB3 and EB1 (EB1 sequence), respectively. Residues highlighted in blue in the EB1 sequence were shown to affect MT association in cells; in gray, residues that do not affect MT binding (Slep and Vale, 2007). (B) X-ray crystal structure of EB3-CH domain (yellow ribbon) overlaid onto the ones of EB1 (green ribbon; PDB entry 1pa7) and Bim1 (magenta ribbon; PDB entry 2qjx). (C and D) Two views of the EB3-CH domain, 150° apart and in surface representation. EB3 residue assignments are indicated. Both panels depict sequence differences between EB3 and EB2 and between EB3 and EB1. The color code is the same as in (A) with the addition that simultaneous residue changes in both EB1 and EB2 are indicated in orange if it is unknown whether they influence MT binding, light orange if they do not affect MT binding, and in purple if they do (Slep and Vale, 2007).

2005). Unexpectedly, these dimers readily exchange their subunits in cells and as purified proteins in vitro. This property seems to be more pronounced for EB1 and EB3, compared with EB2. We show that heterodimerization between EB1 and EB3 occurs at endogenous expression levels; it might increase the structural and functional diversity of the EBs. Subunit exchange between EB dimers also explains why overexpression of the C-terminal EB1 fragment has a dominant-negative effect on the endogenous EBs. Until now, overexpression of the EB1 or EB3 C termini was mainly used as a tool aimed at hindering the interaction between the EBs and their binding partners (Askham et al., 2002; Wen et al., 2004; Zhou et al., 2004; Etienne-Manneville et al., 2005; Geraldo et al., 2008). Our findings indicate that the data obtained by overexpression of these EB fragments must be interpreted with caution because EBs themselves are their primary targets.

By using a combination of approaches we show that in cells EBs (in particular EB1 and EB3) have little effect on MT growth rate or rescues, but suppress catastrophes. This is in line with observations in fission yeast and in *Xenopus* extracts, where EB homologues displayed an anti-catastrophe activity (Tirnauer et al., 2002; Busch and Brunner, 2004). In contrast, in our hands EB3 increases MT growth velocity and promotes both catastrophes and rescues when MT dynamics is reconstituted with purified proteins. An important conclusion of our study is that this change can be brought about by a monomer of a CH domain with an adjacent linker sequence. We favor the idea that EB accumulation changes the structure of the MT tip (des Georges et al., 2008; Vitre et al., 2008), and thus promotes MT growth but also increases the probability of a catastrophe in vitro.

To explain the discrepancy between the in vitro and in vivo results, we propose that the activities measured in these conditions are fundamentally different. This is supported by the fact that the structural requirements for the observed effects are different as well: in cells, only EB3 mutants that form dimers inhibit catastrophes, whereas in a purified system a considerable effect on MT dynamics is produced by monomeric EB3. What we measure in cells is most likely not an intrinsic activity of the EBs, but rather their effect on activities of other MT-regulating factors.

Because the EBs bind to multiple +TIPs, it was important to determine if their catastrophe-suppressing activity depends on direct interactions with any of these factors. Two lines of evidence suggest that this is not the case. First, we have shown that EB1 or EB3 lacking the C-terminal acidic tail essential for interactions with the major EB partners are sufficient to completely restore processive MT growth in EB1/EB3-deficient cells. Second, an artificial EB3 dimer, which lacked the whole

Published March 2, 2009

Table III. **Parameters of MT dynamics in vitro**

	Growth rate	Shortening rate	Catastrophe frequency	Rescue frequency
	μm/min	*μm/min*	*min*$^{-1}$	*min*$^{-1}$
Control	0.50 ± 0.19 *n* = 107	10.37 ± 2.85 *n* = 99	0.13 *n* = 107	0.09 *n* = 4
EB3 (200 nM)	2.36 ± 0.48 *n* = 136	15.50 ± 4.85 *n* = 135	1.17 *n* = 136	0.59 *n* = 11
EB3 (1 μM)	2.56 ± 0.43 *n* = 185	14.18 ± 2.59 *n* = 185	1.00 *n* = 185	0.26 *n* = 9
EB3-GFP (200 nM)	2.75 ± 0.37 *n* = 85	14.67 ± 2.46 *n* = 85	0.76 *n* = 85	0.40 *n* = 9
EB3-GFP (1 μM)	1.93 ± 0.28 *n* = 33	13.57 ± 2.11 *n* = 33	0.97 *n* = 33	0.40 *n* = 2
EB3-NL-mVenus (200 nM)	1.82 ± 0.29 *n* = 84	11.86 ± 2.43 *n* = 84	0.84 *n* = 84	0.54 *n* = 9
EB3- NL-mVenus (1 μM)	1.58 ± 0.27 *n* = 88	10.53 ± 1.83 *n* = 88	0.76 *n* = 88	0.16 *n* = 3

The number of events measured for each condition (*n*) is indicated below each measurement. Growing and shortening rates were determined from kymograph slopes corresponding to individual growth or shrinkage phases. An average rate was determined as an average over all events weighted with the time of individual events (± weighted SD). Transition frequencies were determined as a number of events divided by time spent in the growing or shrinking phase, respectively.

C-terminal partner-binding domain, displayed a significant catastrophe-inhibiting activity.

On the other hand, catastrophe suppression by the EBs in cells is strongly correlated with their capacity to bind MT tips because dimerization and the presence of the linker region have a positive effect on both properties. Furthermore, EB2, which binds MT tips less prominently compared with EB1 and EB3, is also a much less potent inhibitor of catastrophes. In this respect, EB2 behaves similar to monomeric EB3-NL, which is also unable to support processive MT growth or efficiently compete with full-length EB1 and EB3 for the binding sites at MT ends. The relevant differences between EB2 and EB1/EB3 may indeed influence MT binding because they cluster around CH domain residues important for MT plus-end accumulation (Fig. 8, C and D). These results suggest that the EBs suppress catastrophes through an interaction with MTs. The EBs could stabilize contacts between protofilaments or the lattice seam, as previously suggested (Sandblad et al., 2006; Vitre et al., 2008). They could thus counteract the function of MT-destabilizing factors either directly, by occluding binding sites on the MTs, or indirectly, by altering the MT tip structure.

Although in an in vitro reconstitution system the EBs also influence MT growth rate and the frequency of rescues, this seems not to be the case in cells. It should be noted that in our experiments we were unable to achieve a complete depletion of all three EBs; therefore, we cannot exclude that a more complete knockdown would have an effect on these parameters. Still, it is noteworthy that although EB1 and EB3 directly bind to several important MT rescue factors, such as the CLIPs (Komarova et al., 2002a, 2005), they have very little effect on MT rescue. On the other hand, loss of the CLIPs from MT plus-ends does not affect catastrophes (Komarova et al., 2002a). It appears, therefore, that in spite of their direct interaction, the CLIPs and the EBs act on MTs independently, similar to the situation in fission yeast (Wolyniak et al., 2006). The seemingly independent actions of the EBs and the CLIPs ensure low MT catastrophe and high rescue frequencies, thus resulting in persistent MT growth in the cell interior and a strong accumulation of dynamic MT ends near the cell margin. The existence of long and continuous MT tracks facilitates the traffic between the cell center and cell periphery; it also favors the interactions of dynamic MT ends with the cell cortex that is essential for cell polarization and migration.

Materials and methods

Protein and shRNA expression constructs, co-IP, and Western blotting

Human EB3-GFP was described by Stepanova et al. (2003); pSuper-based vectors to knock down EB1, EB2, EB3, and the control vector (expressing luciferase-specific shRNA), EB1 rescue constructs, and the EB2 expression construct (based on mouse cDNAs) were described by Komarova et al. (2005). HA-tagged EB1 deletion mutants were generated by a PCR-based strategy and subcloned into the pEGFP-N1 vector (Clontech Laboratories, Inc.), which was modified by substituting the GFP open reading frame by a triple HA tag. Homodimerization domain FKBP and the rapamycin-derived homodimerizer AP20187 were obtained from Ariad (http://www.ariad.com/wt/page/regulation_kits). Different EB3 constructs and EB2-EB3 chimeras were generated by PCR and cloned into pEGFP-N1 or pEGFP-C1. GFP-EB3ΔAc was generated in pEGFP-C1 with a linker sequence AQAGGSGGAGSGGEGAVDG inserted between GFP and EB3. EB3-NL-mVenus was cloned into pEGFP-N1 from which the GFP open reading frame was removed; mVenus was generated by introducing the A206K mutation (Zacharias et al., 2002) into the Venus-encoding plasmid (a gift of A. Miyawaki; RIKEN, Wako City, Japan). mCherry-α-tubulin (Shaner et al., 2004) was a gift of Dr. R.Tsien (UCSD, La Jolla, CA).

For co-IP experiments COS-1 cells were transfected by the DEAE-dextran method, lysed 2 d after transfection, and the lysates were used for co-IP with anti-HA antibodies as described by Hoogenraad et al. (2000).

Cloning, protein preparation, and SLS analysis

Construction of the bacterial EB1c expression vector is described by Honnappa et al. (2005). Human EB1, EB2c, EB3, and EB3c were PCR-amplified from human EB1, EB2, and EB3 full-length cDNA clones (provided by W. Bu; University of Texas, Houston, TX). Using the Gateway cloning system (Invitrogen) all PCR products were subcloned into a pDONR221 vector by BP reactions and thereafter cloned by LR reactions into a pDEST17 vector according to the manufacturer's instruction. Proteins were expressed in *Escherichia coli* BL21 (DE3) and purified on HiTrap Ni^{2+}-Sepharose chelating columns (GE Healthcare) as described previously (Honnappa et al., 2005). After cleavage of the 6xHIS-tag by thrombin at 4°C overnight, the proteins were gel filtrated on a Superdex-200 column (GE Healthcare) equilibrated in 20 mM Tris-HCl, pH 7.4, 0.15 M NaCl, and 2 mM dithiothreitol. GFP-EB3 and mCherry-EB3 (containing the same linker as GFP-EB3-ΔAc) and EB3-NL-mVenus were subcloned into pET-28a and purified as described above; the 6xHIS-tag was not removed.

Published March 2, 2009

SLS analysis was performed by using a miniDAWN TriStar equipped with an Optilab rEX refractometer (Wyatt Technology corp.), which was coupled to a Superose 12 10/30 (GE Healthcare) size exclusion column run on an Agilent 1100 HPLC. 100 µl of ~1 mg/ml protein solution was injected onto the column equilibrated in 20 mM Tris (pH 7.4), supplemented with 150 mM NaCl. Samples were eluted at a constant flow rate of 0.5 ml/min. The shape-independent molecular masses were determined with the Wyatt Astra v4.90.08 software package.

EB heterodimer formation was monitored by native PAGE analysis following an SDS-free Laemmli system. 100 µM EB protein solutions were mixed in different ratios and incubated for 5 min at 37°C. EBc heterodimers and EBc/EB full-length heterodimers were analyzed at 4°C on 15% and 9% native PAGE gels, respectively.

Crystal structure determination and modeling

EB3 CH domain (1.7 mM; residues 1–130) was crystallized at 20°C by mixing equal volumes (0.2 µl) of protein solution with the reservoir solution (40 mM potassium phosphate, 16% PEG 8000, and 20% glycerol) using the sitting drop method. Synchrotron datasets were collected at the Swiss Light Source (Villigen PSI, Switzerland) protein beam line X06SA on a pixel counting PILATUS 6M detector. X-ray diffraction data were collected at 100 K. Data collection and refinement statistics are given in Table S1 (available at http://www.jcb.org/cgi/content/full/jcb.200807179/DC1). The structure was solved by molecular replacement using a search model based on the crystal structure of the EB1 CH domain (PDB ID code 1PA7).

We failed to crystallize the EB2 CH domain; however, because of the high sequence conservation between the CH domains of EB2 and EB1 (sequence identity and sequence similarity of 77% and 91%, respectively) we modeled the structure of EB2 CH (residues 44–173) using the SWISS-MODEL software package (Arnold et al., 2006) and using the EB1 CH structure (PDP ID 1PA7) as a template. Structural figures were prepared with the program PyMOL (De-Lano Scientific, LLC).

Cell culture, transfection, and microinjection

The CHO-K1 cell line stably expressing YFP-CLIP-170 was described previously (Komarova et al., 2005). To introduce different expression vectors into cells we used microinjection or transient transfection. Cells were plated sparsely on coverslips with photoetched locator grids (Bellco Glass) and 12–24 h later they were microinjected with different shRNA-expressing plasmids into nuclei. The needle concentration was 100 µg/ml for RNAi plasmids and 70 µg/ml for EB expression constructs in the rescue experiments with EB1, EB2, or EB1ΔAc. To observe MT behavior directly we used a CFP-expressing EB1/EB3 shRNA construct (Komarova et al., 2005); CFP-positive cells were microinjected into the cytoplasm with Cy3-labeled tubulin at a needle concentration of 10 mg/ml. Cells were fixed or used for live observation 72–90 h after microinjection. In experiments where cotransfection of shRNA and rescue constructs was used, cells were transfected with FuGene 6 (Roche) at 50% confluence, replated at low density on coverslips 24 h later, and analyzed by live imaging after an additional 72 h in culture.

Antibodies

We used rat monoclonal antibodies KT51, KT52, and KT53 against EB1, EB2, and EB3 proteins (Absea); mouse monoclonal antibodies EB1 and EB3 (BD Biosciences), HA tag (Babco), a rat monoclonal antibody against α-tubulin (YL1/2; Abcam), and rabbit antibodies against EB3 (02–1005-07; Stepanova et al., 2003) and GFP (Abcam and Invitrogen). The following secondary antibodies were used: alkaline phosphatase–conjugated anti–rabbit and anti–mouse antibodies (Sigma-Aldrich), TRITC- and FITC-conjugated donkey anti–mouse and anti–rabbit and Cy5-conjugated anti–rat antibodies (Jackson ImmunoResearch Laboratories).

Immunostaining and analysis of EB protein accumulation at the MT tips

Cell fixation and staining were performed as described previously (Komarova et al., 2002a). Fixed samples were analyzed by fluorescence deconvolution microscopy using a DeltaVision microscope system equipped with an Olympus IX70 inverted microscope and a PlanApo 60x 1.4 NA objective. We used x2 binning that gave a resolution of 0.22 µm/pixel. Images were prepared for presentation using Adobe Photoshop. Analysis of fluorescence intensity distribution of EBs along MT ends was performed using MetaMorph and SigmaPlot software as described by Komarova et al. (2005). In brief, the intensity profiles from different microtubule ends were aligned based on the strong increase in pixel intensity compared with the background (the point where pixel intensity abruptly changed was considered as the microtubule tip). Because line-scan analysis was performed on the combined three-color images (obtained using DeltaVision software) and there was no obvious chromatic shift, the position of the microtubule tip was determined based on the profiles of the expressed EB family members in the case when other members were depleted.

Live imaging, image processing, and quantification of MT dynamics

Microinjected CHO-K1 cells were imaged on the Nikon Diaphot 300 inverted microscope equipped with a Plan 100x, 1.25 N.A. objective and YFP, GFP, and Cy3 filter sets. Cells injected with Cy3-tubulin were treated with the oxygen-depleting preparation, Oxyrase. 16-bit images were collected with a CH350 slow-scan, cooled CCD camera (Photometrics Ltd.) driven by MetaMorph software (MDS Analytical Technologies). The images were projected onto the CCD chip with a resolution of 0.09 µm/pixel. Time-lapse series of 50–150 images were collected at 2–3-s intervals.

For transfection-based experiments, cells were imaged on the inverted Nikon Eclipse TE2000E microscope equipped with a CFI Apo TIRF 100x 1.49 N.A. oil objective (Nikon), equipped with a QuantEM EMCCD camera (Roper Scientific) controlled by MetaMorph software. For excitation we used an HBO 103 W/2 Mercury Short Arc Lamp (Osram) and a Chroma ET-GFP filter cube. Images were collected with ~0.5-s exposure in a stream mode. Total internal reflection fluorescence microscopy (TIRFM) imaging for the in vitro plus-end tracking assay was performed on the same setup, using the 113-mW, 488-nm laser line of an argon laser (Spectra-Physics Lasers) and 11-mW, 561-nm diode-pumped solid-state laser (Melles Griot) for excitation. For separation of emissions we used DualView (Optical Insight) with emitters HQ530/30M and HQ630/50M (Chroma Technology Corp.) and the beam splitter 565DCXR (Chroma Technology Corp.). The 16-bit images were projected onto the CCD chip at a magnification of 0.067 µm/pixel with the intermediate magnification 2.5x. Photobleaching was performed with the same setup using the scanning head FRAP L5 D–CURIE (Curie Institute) and 113-mW 488-nm laser line of argon laser (Spectra-Physics Lasers).

MT dynamics parameters were measured manually using 16-bit images in MetaMorph software; SigmaPlot software was used for statistical analysis and plotting of graphs as described elsewhere (Komarova et al., 2002a,b). MT life histories were plotted as length (µm) versus time (s). Instantaneous growth and shortening rates were calculated as displacement of the growing or shortening plus-ends between successive frames in a time-lapse series for the data presented in Tables I and II and Figs. 2 and 4, and by using kymograph analysis for Fig. S5. Transition frequencies were quantified using YFP-CLIP-170 tracks, direct or subtracted images of labeled MTs (Vorobjev et al., 1999). Quantification of the MT length distribution along the cell radius was performed as described elsewhere (Komarova et al., 2002a,b).

Images were prepared for presentation with Adobe Photoshop by cropping and adjusting contrast and levels. Additional processing is indicated in the figure legends.

In vitro plus-end tracking assay

Plus-end tracking assay was performed as described by Bieling et al. (2007), with some modifications. Flow chambers were assembled between a precleaned glass coverslip and a microscopy slide that were glued together using Dow Corning high vacuum silicone grease (Sigma-Aldrich). The chamber was incubated with 0.2 mg/ml PLL-PEG-biotin (Susos AG) in assay buffer (80 mM K-PIPES, pH 6.8, 4 mM $MgCl_2$, and 1 mM EGTA) and after rinsing with 1 mg/ml streptavidin in the assay buffer. Short MT seeds were prepared by incubation of 30 µM tubulin mix containing 17% biotin-tubulin and 6% rhodamine-tubulin (Cytoskeleton, Inc.), with 1 mM GMPCPP (Jena Bioscience) at 36°C for 20 min. The seeds were diluted 10-fold with 2 µM taxol (Cytoskeleton, Inc.) in assay buffer and further incubated for 10 min at 36°C. We used the same tubulin batch to prepare seeds and in the polymerization mix. The seeds were specifically attached to the functionalized surface by biotin-streptavidin links. The flow chamber was blocked by incubation with 1 mg/ml κ-casein. Accumulation of GFP-tagged +TIPs at the ends of dynamic MTs was observed in the presence of 15 µM tubulin in the assay buffer supplemented with 1 mM GTP, 0.2 mg/ml κ-casein, 0.1% methylcellulose (4000cP; Sigma-Aldrich), and an oxygen scavenger system (50 mM glucose, 400 µg/ml glucose-oxidase, 200 µg/ml catalase, and 4 mM DTT). The samples were sealed with candle wax. During experiments the samples were kept at 26 ± 1°C; images were collected using TIRFM.

Measurement of MT dynamics in vitro using DIC microscopy

MTs were nucleated from seeds (prepared as described above, but without rhodamine-tubulin) bound to the surface of a flow chamber as described above. MT growth was initiated by flowing in a solution containing 15 µM tubulin, 1 mM GTP, and EB3 constructs (at a concentration of 0.2 or 1 µM) in assay buffer supplemented with 50 mM KCl, 0.1% methyl cellulose, 0.3 mg/ml κ-casein, and an oxygen scavenger system. MTs were imaged by video-enhanced DIC microscopy, using an inverted microscope (DMIRB; Leica) equipped with a 100x/1.3 N.A. oil immersion objective (HCX PL

Published March 2, 2009

FLUOTAR; Leica). The temperature in the sample was adjusted and maintained at 25 ± 1°C by Peltier elements (Melcor) mounted on a sleeve around the objective and controlled by in-house built electronics. Images acquired with a CCD camera (CF8/1; Kappa) were further processed for background substraction and contrast enhancement with an image processor (C5510 Argus 20; Hamamatsu Photonics) and digitized on-line at a rate of 1 frame per second (fps) with an in-house developed software (written and run in IDL). Simultaneously with the on-line digitization, the processed images were recorded on a DVD at video rate 25 fps, with a commercial burner (DVD R-80; Philips). Measurements were performed using kymograph analysis in MetaMorph software.

Online supplemental material

Figure S1 demonstrates the effect of EB1-CΔAc overexpression on the accumulation of endogenous EBs at the MT tips. Figure S2 shows the extent of EB1/EB3 depletion after nuclear microinjection, illustrates MT dynamics in a control and an EB1/EB3-deleted cell, and the visualization of MT outgrowth from the centrosome using photobleaching. Figure S3 shows size exclusion chromatography profiles of purified EBs and representative kymographs illustrating MT plus-end dynamics in vitro with and without EB3. Figures S4 and S5 show histograms of MT growth track lengths and the average MT growth rate in different conditions. Videos illustrate MT growth in control and EB1/EB3-depleted cells using YFP-CLIP-170 or Cy3-labeled tubulin, and plus-end tracking behavior of the full-length EB3 and its monomeric N-terminal fragment in vitro. Online supplemental material is available at http://www.jcb.org/cgi/content/full/jcb.200807179/DC1.

We are grateful to Dr. Yuko Mimori-Kiyosue for giving us the idea about designing the dominant negative mutant of EB1 and to Dr. Monica Balsera Dieguez for help with the homology modeling. We thank Ariad (Cambridge, MA), A. Miyawaki (RIKEN, Wako City, Japan), W. Bu (The University of Texas, Houston, TX) and R.Tsien (UCSD, La Jolla, CA) for the gift of materials.

This work was supported by the Netherlands Organization for Scientific Research grants to A.A., by Fundação para a Ciência e a Tecnologia fellowship to S.M. Gouveia, by a FEBS fellowship to R.M. Buey, by the National Institutes of Health grant GM25062 to G.G. Borisy and by the Swiss National Science Foundation through grant 3100A0-109423 and by the National Center of Competence in Research Structural Biology program to M.O. Steinmetz.

Submitted: 30 July 2008
Accepted: 4 February 2009

References

Akhmanova, A., and M.O. Steinmetz. 2008. Tracking the ends: a dynamic protein network controls the fate of microtubule tips. *Nat. Rev. Mol. Cell Biol.* 9:309–322.

Arnold, K., L. Bordoli, J. Kopp, and T. Schwede. 2006. The SWISS-MODEL workspace: a web-based environment for protein structure homology modelling. *Bioinformatics.* 22:195–201.

Askham, J.M., K.T. Vaughan, H.V. Goodson, and E.E. Morrison. 2002. Evidence that an interaction between EB1 and p150(Glued) is required for the formation and maintenance of a radial microtubule array anchored at the centrosome. *Mol. Biol. Cell.* 13:3627–3645.

Bieling, P., L. Laan, H. Schek, E.L. Munteanu, L. Sandblad, M. Dogterom, D. Brunner, and T. Surrey. 2007. Reconstitution of a microtubule plus-end tracking system in vitro. *Nature.* 450:1100–1105.

Bieling, P., S. Kandels-Lewis, I.A. Telley, J. van Dijk, C. Janke, and T. Surrey. 2008. CLIP-170 tracks growing microtubule ends by dynamically recognizing composite EB1/tubulin-binding sites. *J. Cell Biol.* 183:1223–1233.

Busch, K.E., and D. Brunner. 2004. The microtubule plus end-tracking proteins mal3p and tip1p cooperate for cell-end targeting of interphase microtubules. *Curr. Biol.* 14:548–559.

des Georges, A., M. Katsuki, D.R. Drummond, M. Osei, R.A. Cross, and L.A. Amos. 2008. Mal3, the *Schizosaccharomyces pombe* homolog of EB1, changes the microtubule lattice. *Nat. Struct. Mol. Biol.* 15:1102–1108.

Desai, A., and T.J. Mitchison. 1997. Microtubule polymerization dynamics. *Annu. Rev. Cell Dev. Biol.* 13:83–117.

Dixit, R., B. Barnett, J.E. Lazarus, M. Tokito, Y.E. Goldman, and E.L. Holzbaur. 2009. Microtubule plus-end tracking by CLIP-170 requires EB1. *Proc. Natl. Acad. Sci. USA.* 106:492–497.

Dragestein, K.A., W.A. van Cappellen, J. van Haren, G.D. Tsibidis, A. Akhmanova, T.A. Knoch, F. Grosveld, and N. Galjart. 2008. Dynamic behavior of GFP-CLIP-170 reveals fast protein turnover on microtubule plus ends. *J. Cell Biol.* 180:729–737.

Etienne-Manneville, S., J.B. Manneville, S. Nicholls, M.A. Ferenczi, and A. Hall. 2005. Cdc42 and Par6-PKCzeta regulate the spatially localized association of Dlg1 and APC to control cell polarization. *J. Cell Biol.* 170:895–901.

Geraldo, S., U.K. Khanzada, M. Parsons, J.K. Chilton, and P.R. Gordon-Weeks. 2008. Targeting of the F-actin-binding protein drebrin by the microtubule plus-tip protein EB3 is required for neuritogenesis. *Nat. Cell Biol.* 10:1181–1189.

Hayashi, I., and M. Ikura. 2003. Crystal structure of the amino-terminal microtubule-binding domain of end-binding protein 1 (EB1). *J. Biol. Chem.* 278:36430–36434.

Hayashi, I., A. Wilde, T.K. Mal, and M. Ikura. 2005. Structural basis for the activation of microtubule assembly by the EB1 and p150Glued complex. *Mol. Cell.* 19:449–460.

Honnappa, S., C.M. John, D. Kostrewa, F.K. Winkler, and M.O. Steinmetz. 2005. Structural insights into the EB1-APC interaction. *EMBO J.* 24:261–269.

Hoogenraad, C.C., A. Akhmanova, F. Grosveld, C.I. De Zeeuw, and N. Galjart. 2000. Functional analysis of CLIP-115 and its binding to microtubules. *J. Cell Sci.* 113:2285–2297.

Howard, J., and A.A. Hyman. 2003. Dynamics and mechanics of the microtubule plus end. *Nature.* 422:753–758.

Juwana, J.P., P. Henderikx, A. Mischo, A. Wadle, N. Fadle, K. Gerlach, J.W. Arends, H. Hoogenboom, M. Pfreundschuh, and C. Renner. 1999. EB/RP gene family encodes tubulin binding proteins. *Int. J. Cancer.* 81:275–284.

Kita, K., T. Wittmann, I.S. Nathke, and C.M. Waterman-Storer. 2006. Adenomatous polyposis coli on microtubule plus ends in cell extensions can promote microtubule net growth with or without EB1. *Mol. Biol. Cell.* 17:2331–2345.

Komarova, Y.A., A.S. Akhmanova, S. Kojima, N. Galjart, and G.G. Borisy. 2002a. Cytoplasmic linker proteins promote microtubule rescue in vivo. *J. Cell Biol.* 159:589–599.

Komarova, Y.A., I.A. Vorobjev, and G.G. Borisy. 2002b. Life cycle of MTs: persistent growth in the cell interior, asymmetric transition frequencies and effects of the cell boundary. *J. Cell Sci.* 115:3527–3539.

Komarova, Y., G. Lansbergen, N. Galjart, F. Grosveld, G.G. Borisy, and A. Akhmanova. 2005. EB1 and EB3 control CLIP dissociation from the ends of growing microtubules. *Mol. Biol. Cell.* 16:5334–5345.

Louie, R.K., S. Bahmanyar, K.A. Siemers, V. Votin, P. Chang, T. Stearns, W.J. Nelson, and A.I. Barth. 2004. Adenomatous polyposis coli and EB1 localize in close proximity of the mother centriole and EB1 is a functional component of centrosomes. *J. Cell Sci.* 117:1117–1128.

Manna, T., S. Honnappa, M.O. Steinmetz, and L. Wilson. 2007. Suppression of microtubule dynamic instability by the +TIP protein EB1 and its modulation by the CAP-Gly domain of p150(Glued). *Biochemistry.* 47:779–786.

Mimori-Kiyosue, Y., I. Grigoriev, G. Lansbergen, H. Sasaki, C. Matsui, F. Severin, N. Galjart, F. Grosveld, I. Vorobjev, S. Tsukita, and A. Akhmanova. 2005. CLASP1 and CLASP2 bind to EB1 and regulate microtubule plus-end dynamics at the cell cortex. *J. Cell Biol.* 168:141–153.

Rehberg, M., and R. Graf. 2002. *Dictyostelium* EB1 is a genuine centrosomal component required for proper spindle formation. *Mol. Biol. Cell.* 13:2301–2310.

Rogers, S.L., G.C. Rogers, D.J. Sharp, and R.D. Vale. 2002. *Drosophila* EB1 is important for proper assembly, dynamics, and positioning of the mitotic spindle. *J. Cell Biol.* 158:873–884.

Sandblad, L., K.E. Busch, P. Tittmann, H. Gross, D. Brunner, and A. Hoenger. 2006. The *Schizosaccharomyces pombe* EB1 homolog Mal3p binds and stabilizes the microtubule lattice seam. *Cell.* 127:1415–1424.

Schroder, J.M., L. Schneider, S.T. Christensen, and L.B. Pedersen. 2007. EB1 is required for primary cilia assembly in fibroblasts. *Curr. Biol.* 17:1134–1139.

Schuyler, S.C., and D. Pellman. 2001. Microtubule "plus-end-tracking proteins": The end is just the beginning. *Cell.* 105:421–424.

Shaner, N.C., R.E. Campbell, P.A. Steinbach, B.N. Giepmans, A.E. Palmer, and R.Y. Tsien. 2004. Improved monomeric red, orange and yellow fluorescent proteins derived from *Discosoma sp.* red fluorescent protein. *Nat. Biotechnol.* 22:1567–1572.

Slep, K.C., and R.D. Vale. 2007. Structural basis of microtubule plus end tracking by XMAP215, CLIP-170, and EB1. *Mol. Cell.* 27:976–991.

Slep, K.C., S.L. Rogers, S.L. Elliott, H. Ohkura, P.A. Kolodziej, and R.D. Vale. 2005. Structural determinants for EB1-mediated recruitment of APC and spectraplakins to the microtubule plus end. *J. Cell Biol.* 168:587–598.

Stepanova, T., J. Slemmer, C.C. Hoogenraad, G. Lansbergen, B. Dortland, C.I. De Zeeuw, F. Grosveld, G. van Cappellen, A. Akhmanova, and N. Galjart. 2003. Visualization of microtubule growth in cultured neurons via the use of EB3-GFP (end-binding protein 3-green fluorescent protein). *J. Neurosci.* 23:2655–2664.

Straube, A., and A. Merdes. 2007. EB3 regulates microtubule dynamics at the cell cortex and is required for myoblast elongation and fusion. *Curr. Biol.* 17:1318–1325.

Su, L.K., and Y. Qi. 2001. Characterization of human MAPRE genes and their proteins. *Genomics.* 71:142–149.

Tirnauer, J.S., and B.E. Bierer. 2000. EB1 proteins regulate microtubule dynamics, cell polarity, and chromosome stability. *J. Cell Biol.* 149:761–766.

Tirnauer, J.S., E. O'Toole, L. Berrueta, B.E. Bierer, and D. Pellman. 1999. Yeast Bim1p promotes the G1-specific dynamics of microtubules. *J. Cell Biol.* 145:993–1007.

Tirnauer, J.S., S. Grego, E.D. Salmon, and T.J. Mitchison. 2002. EB1-microtubule interactions in *Xenopus* egg extracts: role of EB1 in microtubule stabilization and mechanisms of targeting to microtubules. *Mol. Biol. Cell.* 13:3614–3626.

Vitre, B., F.M. Coquelle, C. Heichette, C. Garnier, D. Chretien, and I. Arnal. 2008. EB1 regulates microtubule dynamics and tubulin sheet closure in vitro. *Nat. Cell Biol.* 10:415–421.

Vorobjev, I.A., V.I. Rodionov, I.V. Maly, and G.G. Borisy. 1999. Contribution of plus and minus end pathways to microtubule turnover. *J. Cell Sci.* 112(Pt 14):2277–2289.

Weisbrich, A., S. Honnappa, R. Jaussi, O. Okhrimenko, D. Frey, I. Jelesarov, A. Akhmanova, and M.O. Steinmetz. 2007. Structure-function relationship of CAP-Gly domains. *Nat. Struct. Mol. Biol.* 14:959–967.

Wen, Y., C.H. Eng, J. Schmoranzer, N. Cabrera-Poch, E.J. Morris, M. Chen, B.J. Wallar, A.S. Alberts, and G.G. Gundersen. 2004. EB1 and APC bind to mDia to stabilize microtubules downstream of Rho and promote cell migration. *Nat. Cell Biol.* 6:820–830.

Wolyniak, M.J., K. Blake-Hodek, K. Kosco, E. Hwang, L. You, and T.C. Huffaker. 2006. The Regulation of microtubule dynamics in *S. cerevisiae* by three interacting plus-end tracking proteins. *Mol. Biol. Cell.* 17:2789–2798.

Yan, X., R. Habedanck, and E.A. Nigg. 2006. A complex of two centrosomal proteins, CAP350 and FOP, cooperates with EB1 in microtubule anchoring. *Mol. Biol. Cell.* 17:634–644.

Zacharias, D.A., J.D. Violin, A.C. Newton, and R.Y. Tsien. 2002. Partitioning of lipid-modified monomeric GFPs into membrane microdomains of live cells. *Science.* 296:913–916.

Zhou, F.Q., J. Zhou, S. Dedhar, Y.H. Wu, and W.D. Snider. 2004. NGF-induced axon growth is mediated by localized inactivation of GSK-3beta and functions of the microtubule plus end binding protein APC. *Neuron.* 42:897–912.

Published March 2, 2009

Komarova et al., http://www.jcb.org/cgi/content/full/jcb.200807179/DC1

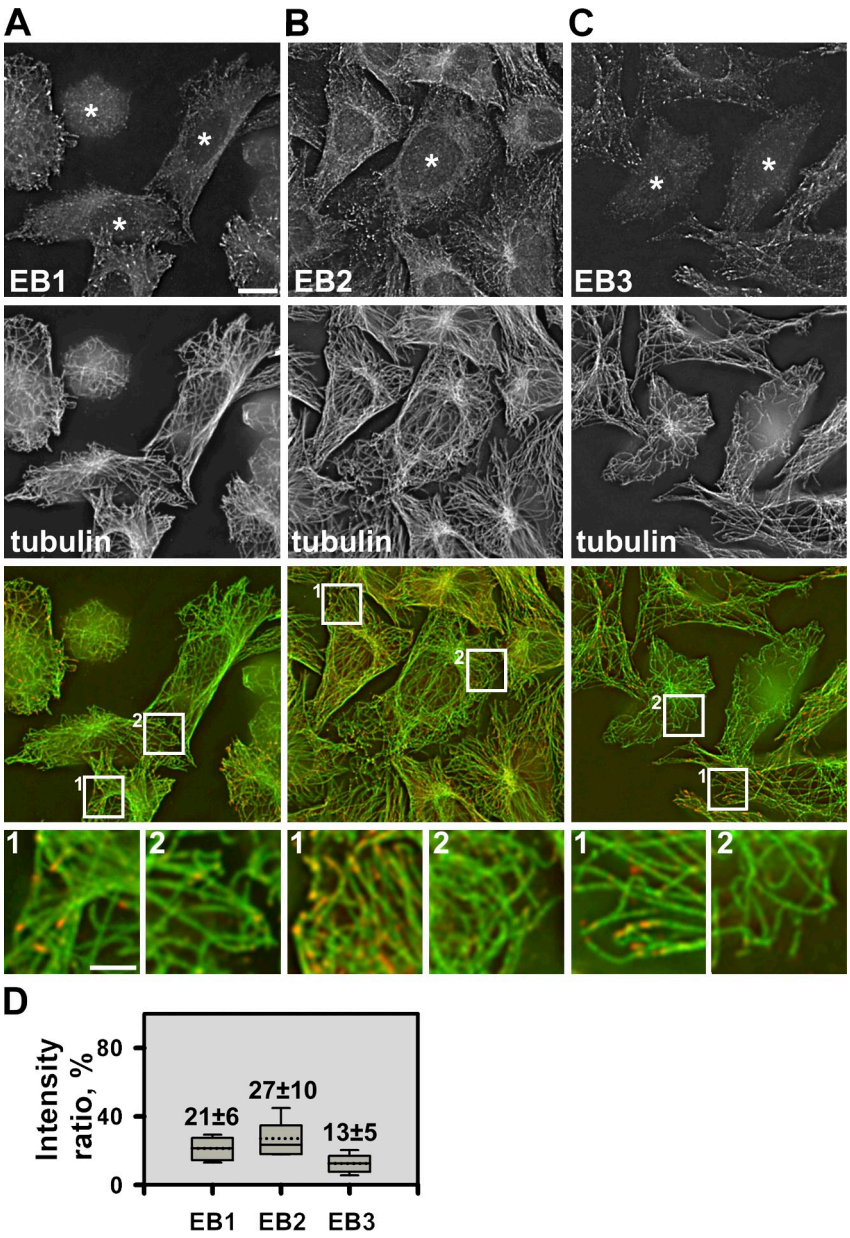

Figure S1. **Expression of EB1-CΔAc reduces the accumulation of endogenous EBs at the MT tips.** (A–C) CHO-K1 cells expressing HA-EB1-CΔAc mutant were stained for the HA tag to detect expressing cells (indicated by asterisks) for endogenous EB1 (A), EB2 (B), and EB3 (C) (red) and tubulin (green). Cells expressing HA-EB1-CΔAc mutant showed reduced levels of EBs at the MT tips. Bar, 10 μm. Enlarged parts of the non-transfected cells (box 1) and cells expressing HA-EB1-CΔAc mutant (box 2) are shown in the panels beneath. Bar, 5 μm. (D) Quantification of the accumulation of EBs at the outmost MT tips in the cells expressing HA-EB1-CΔAc mutant. Integrated intensity of EB1, EB2, and EB3 was expressed as a percentage of the intensity in control cells from the same image, which was taken for 100%. The boundaries of the box and whiskers indicate the 25th and the 75th percentile, and the 90th and 10th percentiles, respectively. The median and the mean are shown by a straight and a dotted line, respectively. Numbers on the graphs indicate the average percentage ± SD of the signal remaining at the MT tips.

Published March 2, 2009

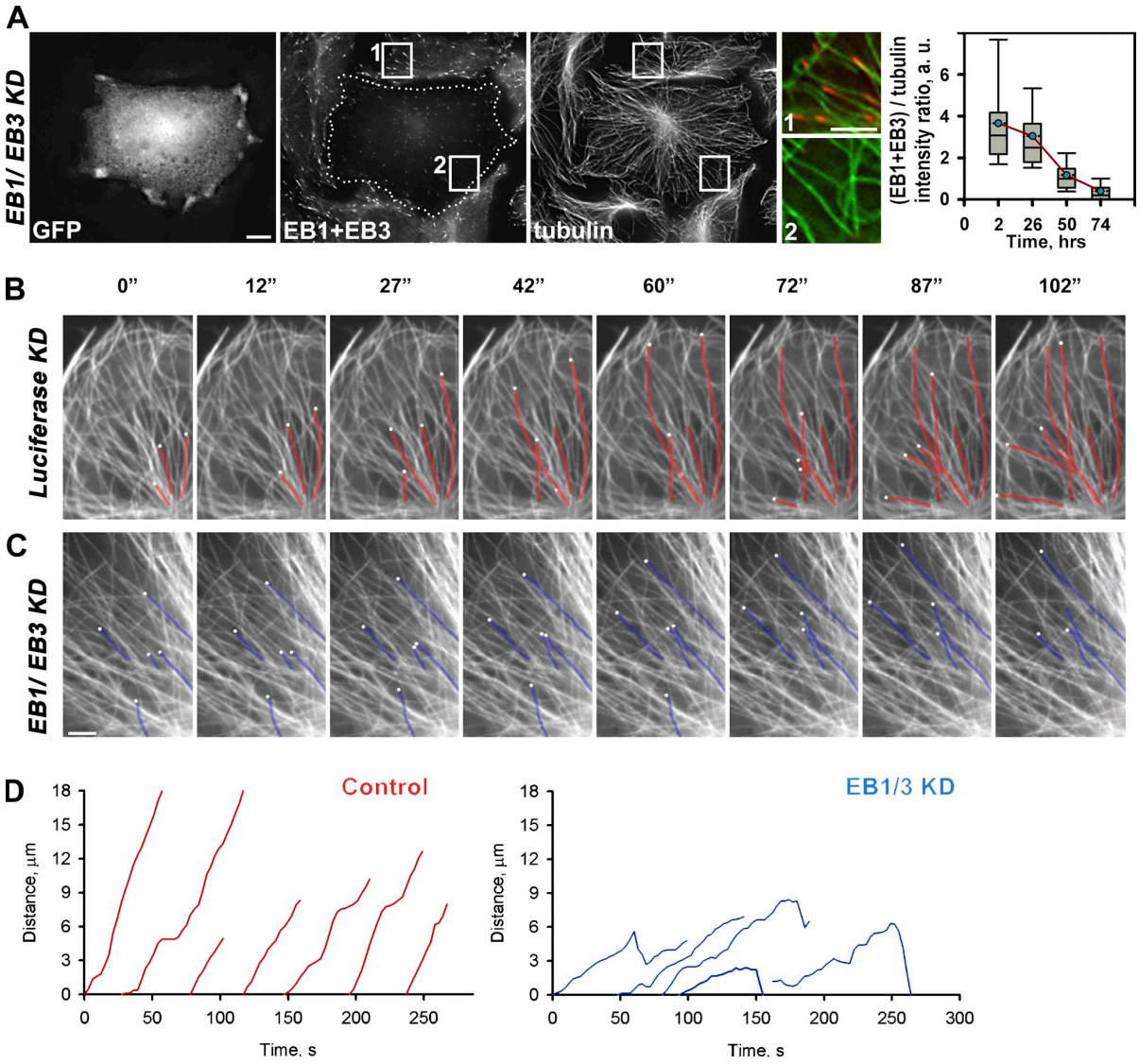

Figure S2. **Characterization of EB1/EB3-depleted cells.** (A) Simultaneous depletion of EB1 and EB3 by nuclear microinjection. A representative image of CHO-K1 cells stained for GFP, EB1 + EB3 (mixture of antibodies), and tubulin 74 h after microinjection of CFP-expressing EB1/EB3 shRNA vector. The depleted cell is indicated by a dotted line. Enlarged parts of the control and knockdown cells are shown in color; EB1 + EB3 = red; tubulin = green. Bar, 10 μm. Box graph demonstrating the intensity ratios of EB1 + EB3 to tubulin at the MT tips 2, 26, 50, and 74 h after microinjection of the shRNA construct is shown on the right. The boundaries of the box and whiskers indicate the 25th and the 75th percentile, and the 90th and 10th percentiles, respectively. The median and the mean are shown by straight lines and blue circles, respectively. The levels of the remaining EB1 + EB3 proteins expressed as a percentage of the intensity in control cells (taken as 100%) was 100 ± 11% at 2 h (114 MT tips in 13 cells), 82.42 ± 11% at 26 h (141 MT tips in 10 cells), 41± 17% at 50 h (284 MT tips in 14 cells), and at 8.8 ± 2.8% 74 h (221 MT tips in 9 cells). In all cases 95% confidence intervals are non-overlapping. (B–D) MT dynamics in CHO-K1 cells after simultaneous depletion of EB1 and EB3. (B and C) CHO-K1 cells co-expressing CFP and luciferase (A) or EB1/EB3 shRNAs (B) were microinjected with Cy3-labeled tubulin and imaged with a 3-s time interval. Several growing MTs are outlined in red (control) or blue (EB1/EB3 depletion); the position of MT plus-ends is indicated by white dots. Bar, 5 μm. (D) Representative MT life history plots (displacement of the plus-end over time) from the cells shown in B and C. (E) Visualization of MT outgrowth from the centrosome using photobleaching. Time-lapse images of a CHO-K1 cell expressing mCherry–α-tubulin before and after photobleaching (photobleached area is outlined by blue line). Several MTs growing from the centrosome are highlighted in red. Time after photobleaching is in the top left corner. Bar 5 μm.

Published March 2, 2009

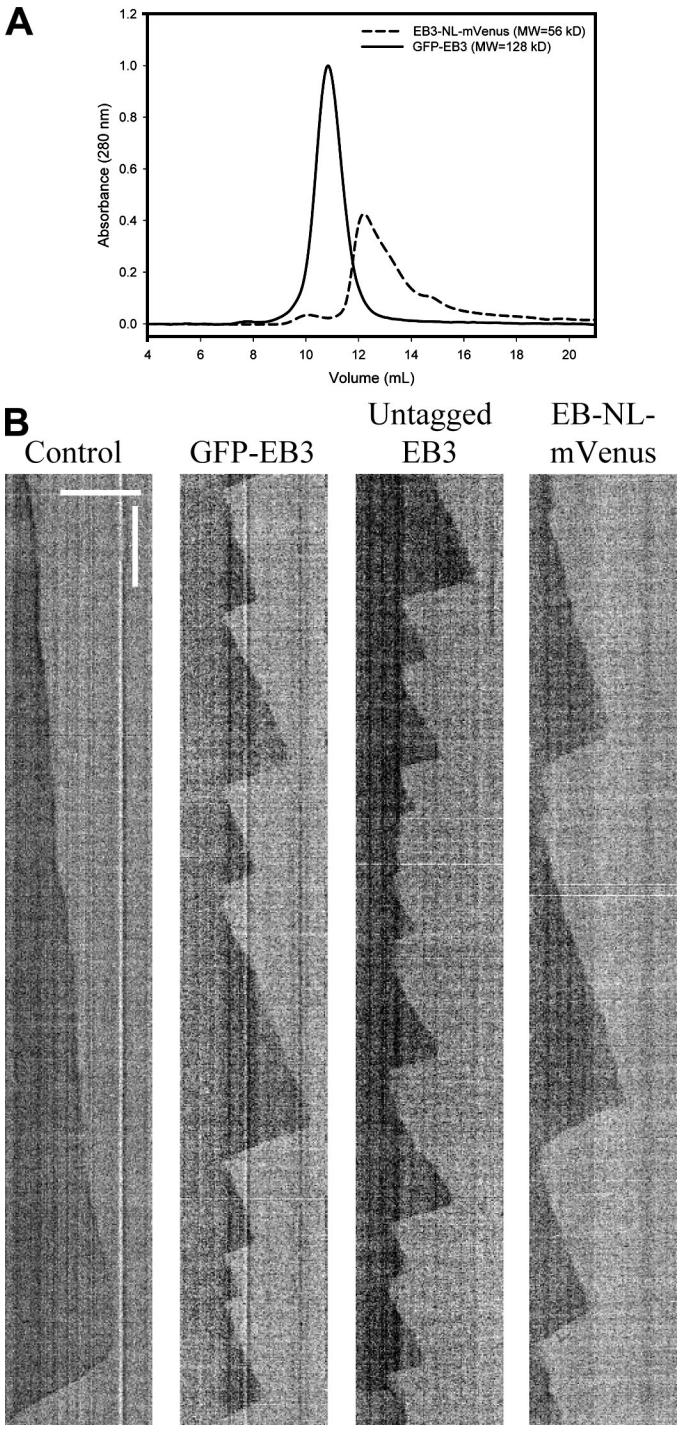

Figure S3. **Analysis of purified EB3 proteins by size-exclusion chromatography and MT dynamics in vitro.** (A) Size exclusion chromatograms of the monomeric and dimeric versions of EB3. Protein elution was monitored by absorbance at 280 nm. The protein mass of the eluted peaks was estimated by static light scattering and is indicated in the plot legend. (B) Representative kymographs of MT plus-end behavior in vitro. Different EB3 mutants (as indicated) were added to 15 μM of tubulin (control) at the concentration of 1 μM. Horizontal bar, 5 μm; vertical bar, 1 min.

Published March 2, 2009

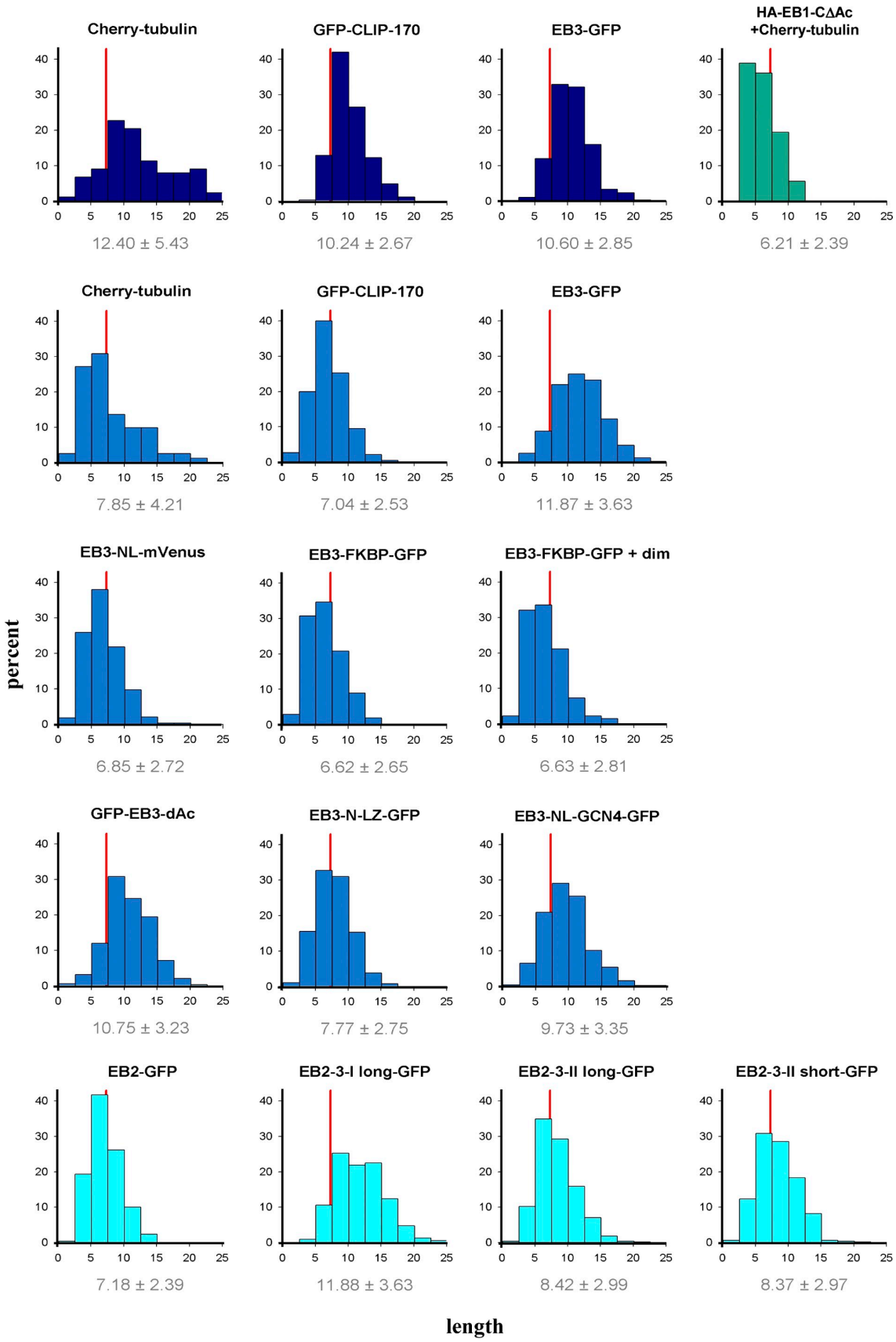

Figure S4. **Histograms of distribution of MT growth lengths in control cells, EB1/EB3-depleted cells, and after rescue with different EB3 and EB2 mutants.** The distributions of MT growth lengths that were used for calculation of the percentage of MT growth episodes longer than for 7.5 μm (red lines) presented in Fig. 7. The color code is the same as for Fig. 7. The average growth length (±SD) for each condition is indicated below the histogram.

Published March 2, 2009

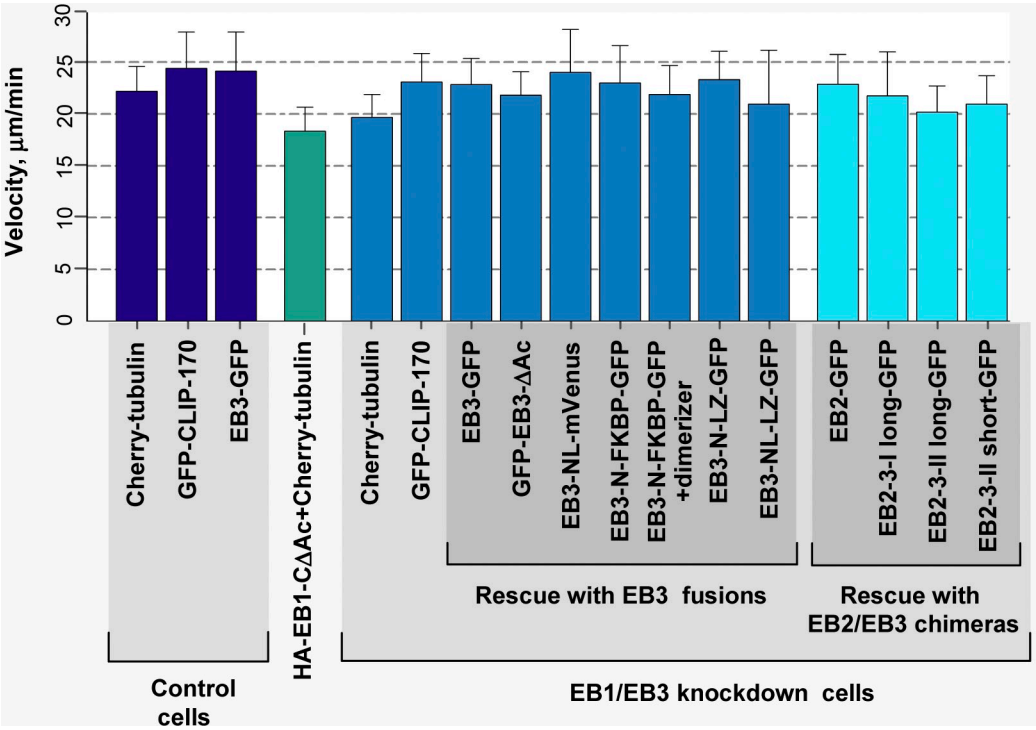

Figure S5. **MT growth rate in control cells, EB1/EB3-depleted cells, and after rescue with different EB3 and EB2 mutants.** MT growth rate was measured using kymographs with the same dataset as in Fig. 7. 180–600 growing MTs were analyzed for each condition. The variation between rates observed in rescue experiments is within the limits of variation between different control experiments. Error bars represent SD.

Table S1. **Crystallography data collection and refinement statistics**

	EB3n
Wavelength, Å	1.0009
Space group (No.)	P21 21 2 (18)
Resolution range, Å	50-1.4
Unit cell, *a*, *b*, and *c* in Å	47.2, 85.4, 32.2
No. of observed reflections	147682 (25226)*
No. of unique reflections	25525 (4469)*
R_{sym}[a], %	10.7 (63.2)*
I/σ (I)	10.9 (3.7)*
Completeness, %	96.9 (92.9)*
No. of refined atoms	
Proteins	1097
Water	151
R-factor/free *R*-factor[b]	0.20/0.23
RMSD bond lengths/bond angles[c]	0.01/1.1

[a] $R_{sym} = \sum_h\sum_i | I_i(h) - \langle I(h)\rangle | \,/\!/\, \sum_h\sum_i I_i(h)$, where $I_i(h)$ and $\langle I(h)\rangle$ are the ith and mean measurement of the intensity of reflection h.
[b] $R = \sum | F_P^{obs} - F_P^{calc} | \,/\!/\, \sum F_P^{obs}$, where F_P^{obs} and F_P^{calc} are the the observed and calculated structure factor amplitudes, respectively.
[c] RMSD, root-mean-square-deviation from the parameter set for ideal stereochemistry.
*Figures in parentheses indicate the values for the outer shell of the data.